1-1-2012

Dynamic Finite Element Modelling And Free Vibration Analysis Of Delaminated Composite Beams

Nicholas Erdelyi
Ryerson University

DYNAMIC FINITE ELEMENT MODELLING AND FREE VIBRATION ANALYSIS OF DELAMINATED COMPOSITE BEAMS

By

Nicholas Erdelyi, B.Eng

Bachelor of Engineering

Ryerson University, 2010

A thesis

presented to Ryerson University

in partial fulfillment of the

requirements for the degree of

Master of Applied Science

in the Program of

Aerospace Engineering

Toronto, Ontario, Canada, 2012

AUTHOR'S DECLARATION

AUTHOR'S DECLARATION FOR ELECTRONIC SUBMISSION OF A THESIS

I hereby declare that I am the sole author of this thesis. This is a true copy of the thesis, including any required final revisions, as accepted by my examiners.

I authorize Ryerson University to lend this thesis to other institutions or individuals for the purpose of scholarly research.

I further authorize Ryerson University to reproduce this thesis by photocopying or by other means, in total or in part, at the request of other institutions or individuals for the purpose of scholarly research.

I understand that my thesis may be made electronically available to the public.

Abstract

Dynamic Finite Element Modelling and Free Vibration Analysis of Delaminated Composite Beams

Nicholas Erdelyi, Master of Applied Science, Aerospace Engineering
Ryerson University, Toronto, 2012

The requirement for accurate analysis tools to predict the behaviour of delaminated composites has grown and will continue to grow into the future, due to the high demand of these materials on major structural components. In the following, a detailed analysis of single- and double-delaminated beams is made, using traditional finite element techniques, as well as two dynamic element-based techniques. The Dynamic Stiffness Matrix (DSM) and Dynamic Finite Element (DFE) techniques introduce the concept of frequency-dependent stiffness matrices and shape functions, respectively, and have been documented to exhibit excellent convergence qualities when compared to traditional finite elements. Current trends in the literature are critically examined, and insight into different types of modeling techniques and constraint types are introduced. In particular, the continuity (both kinematic and force) conditions at delamination tips plays a large role in each model's formulation. In addition, the data previously available from a commercial finite element suite are also utilized to validate the natural frequencies of the systems analyzed here. Beam element-based techniques are used and the results are compared to those obtained using the dynamic element techniques and data from the literature. In each case excellent agreement between different techniques was observed. Finally, general concluding remarks are made on the usefulness of the presented theories, and some comments are made on the future work of this research path.

Acknowledgements

I would like to thank my family and friends for all of their unwavering support along this journey.

I would also like to thank Dr. Hashemi for his unending patience, wisdom, and guidance throughout my research, as well as his encouragement and understanding when I needed them.

Table of Contents

List of Tables

List of Figures

List of Figures (cont'd)

List of Appendices

Nomenclature

i	Beam segment number
x_i	Axial coordinate of beam segment *i*
L_i	Length of beam segment *i*
ξ	x/L
$\overline{W}_i$	Actual transverse displacement
w_i	Assumed transverse displacement
W_i	Frequency-domain magnitude of w_i
ω	Circular frequency of excitation
EI_i	Bending stiffness of beam segment *i*
EA_i	Axial stiffness of beam segment *i*
ρ_i	Mass per unit length of beam segment *i*
A_i	Cross-sectional area of beam segment *i*
a	Delamination length
λ	Non-dimensional frequency $\lambda^2 = \frac{\omega^2 \rho A}{EI} L^4$
$(\cdot)'$	$\frac{d(\cdot)}{dx}$
M	Bending moment
S	Shear force
P	Axial force
$\{\cdot\}$	Column vector
$\langle\cdot\rangle$	Row vector
$[\cdot]$	2-dimensional matrix
$\boldsymbol{F}$	Column vector of nodal forces
$\boldsymbol{K}$	Stiffness matrix
$\boldsymbol{u}$	Column vector of nodal displacements

1. Introduction

Layered structures have seen greatly increased use in civil, shipbuilding, mechanical and aerospace structural applications in recent decades, primarily due to their many attractive features, such as high specific stiffness, high specific strength, good buckling resistance, and formability into complex shapes, to name a few. The replacement of traditionally metallic structural components with laminated composites has resulted in new and unique design challenges. Metallic structures exhibit mainly isotropic material properties and failure modes. By contrast, sandwich/composite materials are anisotropic, which can result in more complex failure modes. Delamination is a common failure mode in layered structures. It may arise from manufacturing defects, loss of adhesion between two layers of the structure, from interlaminar stresses arising from geometric or material discontinuities, or from mechanical loadings. The presence of delamination may significantly reduce the stiffness and strength of the structures. A reduction in the stiffness will affect the vibration characteristics of the structures, such as the natural frequencies and mode shapes. Changes in the natural frequency, as a direct result of the reduction of stiffness, may lead to resonance if the reduced frequency is close to an excitation frequency.

The dynamic modeling of flexible delaminated multi-layer beams has been a topic of interest for many researchers. With the increased use of laminated composite structures, the requirement for accurate delamination models has also grown. The most common delamination models, first formulated in the 1980s [49], dealt with the vibration of two-layer sandwich beams, where layers were governed by the Euler-Bernoulli bending beam theory. The upper and lower intact portions of the delaminated segment were assumed to vibrate freely – independent of each other; as a result this model is known as 'free mode' delamination. It was later discovered that the free mode under-predicted natural frequencies for off-midplane delaminations due to unrestricted penetration of the beams into each other. This was accounted for in 1988 by Mujumdar [35] by constraining the transverse displacements of the top and bottom beams to be equal. The resulting model, known as the 'constrained mode' delamination model, predicts vibration behaviour much more accurately for off-

midplane delamination. However, in modeling terms, the constrained mode implementation results in additional system constraints, leading to increased system stiffness and a possible over-prediction of natural frequencies. As well, the ability to capture opening delamination modes – where the layers separate from each other – which is commonly seen in experimental analysis [31, 43, 47], is lost when using the constrained model. Thus, in the work to follow, the free delamination model will be utilized. Another result of Mujumdar's work [35] was the rigid connector assumption. The assumption states that, for the beam models presented, the delamination faces, which are planar and normal to the neutral axis of the undeformed beam, remain planar (and normal) to the neutral axis of the deformed beam. This assumption, visualized in Figure 1, produces a set of kinematic and force continuity conditions at the delamination tips. It is also worth noting that, in general, a laminated composite beam may have orthotropic, layer-wise material properties, resulting in displacement coupling behaviour. The model used in this work assumes an isotropic or homogenized material, and is not immediately applicable to fibre-reinforced laminated composite beams with arbitrary lay-up patterns, as there would, in general, be a torsional and/or extensional response coupled with flexural vibration [20-22]. Work on extending the presented theory to include these effects has begun, and will be a topic for future research.

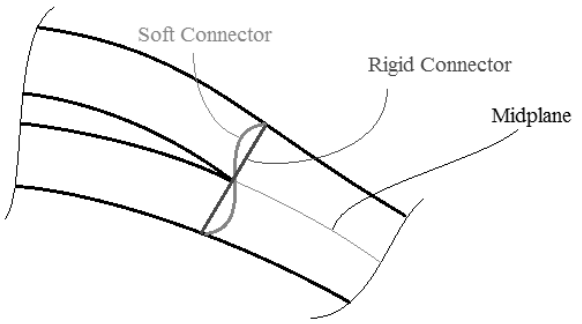

Figure 1 – Soft and rigid delamination connectors for a through-width midplane delamination. The originally planar delamination faces are visualized post-deformation.

The accuracy of vibration analysis and forced response calculation of a flexible structure depends greatly on the reliability of the modal analysis method used and the resulting natural frequencies and modes. There are various analytical, semi-analytical and numerical methods to

predict the natural frequencies and mode shapes of such a system. Several exact solution methods exist for well-defined systems, such as delaminated uniform isotropic beams with constant geometric and material properties. Single [13, 14, 16, 45, 47], multiple [17, 44], and various overlapping and enveloped [15] delamination conditions in space and on various elastic media, such as Pasternak soil [23] have been studied using analytical solution methods. Some work has also been done on delaminated sandwich structures [24], albeit with some mathematical simplification. These solution methods generally use the same procedure as Mujumdar [35] to formulate the kinematic continuity conditions across the delamination tips. The power of this type of formulation lies in the ability to be applied to any number of different system configurations. However, a potential drawback to this procedure is that the system equation must be re-formulated after any configuration change, potentially limiting its applicability.

The conventional Finite Element Method (FEM) has a long, well-established history and is one of the most commonly used methods for modal analysis. The FEM is a general systematic approach to formulate the element mass and stiffness matrices, which are constant in the frequency domain, for a given system. FEM is easily adaptable to complex systems containing variations in geometry or loading through the use of particular modelling techniques. Non-uniform geometry, for example, is often modeled as a stepped, piecewise-uniform configuration. With the method of weighted residuals and Galerkin finite element formulation, the exact variation of the geometry, material properties can also be modeled directly in the formulation [19]. Conventional FEM formulation, based on polynomial shape functions, leads to constant mass and stiffness matrices and results in a linear eigenvalue problem from which the natural frequencies and modes of the system can be readily extracted. One of the advantages of FEM is that one could use Lagrange multipliers to enforce continuity conditions. Although these formulations show good agreement [37] with experimental values, they introduce extra computational overhead by inflating the size of the element matrices, whereas an element developed with the constraints in the formulation would produce results with similar agreement – shown in [30], [29] including axial compression and [25], where a similar technique for delaminated plates was shown– but with a smaller solution domain. The results

would not be strictly identical, since including the conditions explicitly in the formulation enforces them explicitly (exactly equal to zero), while the accuracy of the conditions imposed using the Lagrange multiplier technique would be subject to convergence criteria (suitably close to zero to assume convergence has been obtained).

Other FEM techniques use layerwise theory [28], wherein delamination is represented by the reduction in stiffness of the cross-sections of the beam where the delamination exists, depending on the number of delaminations present and hence, the number of layers which compose the region. The benefit of this type of formulation is that it can model multiple delaminations easily, but the elements are very problem-specific. Rather than discretizing the system into multiple beams and applying delamination conditions to the endpoints of those beams in order to satisfy continuity conditions, this method produces an element for each spanwise location of the beam. This somewhat limits the usefulness of the technique, as a library of different element types would have to be developed for each delamination scenario, rather than simply the application of different boundary conditions to different beam sections.

Another avenue of FEM analysis has been the static analysis of delaminated beams. Although an understanding of dynamic properties of defective composites is important and is the focus of the work presented here, an adequate understanding of composite behaviour in all regimes has been an important focus of academic research by many. For example, FEM formulations based on the principle of virtual work have shown excellent agreement with existing analytical techniques. These modeling techniques, which assume certain kinematics and continuity conditions about the delamination condition, develop equations for the strain energy of the system, either homogenized [40] or using laminated material relationships [39]. Some work has also been done to incorporate shear deformation and rotary inertia into the formulation [41], although the continuity conditions were incorporated using a technique similar to Lagrange multipliers, rather than directly in the formulation. For non-slender beams, this technique showed excellent agreement with a reference FE solution, also noting that the formulation was free of shear-locking, which was shown to cause poor convergence characteristics with high connection stiffness [41]. Most static techniques employ non-linear

methods to ensure the delaminated beam sections do not inter-penetrate each other. Such non-linearities are not able to be resolved into the frequency domain and thus are unsuitable for dynamic analysis without modification, but the use of the principle of virtual work and the application of continuity conditions at the delamination tips are areas of crossover between the dynamic and static FE formulations.

Alternatively, semi-analytical formulations, such as the Dynamic Finite Element (DFE) method [19-22], can be used to carry out structural modal analysis. DFE formulation results in a more accurate prediction method than traditional and FEM modeling techniques, allowing for a reduced mesh size. The main principle of the DFE is the weighted residual integral formulation, which provides a general systematic modeling procedure. The word *dynamic* in DFE acronym refers to the frequency-dependent basis/shape functions of approximation space used to express the displacements, which in turn lead to the *dynamic* stiffness matrix of the system. These shape functions are derived from the general solution to a subset of the differential equations of motion, rather than arbitrary polynomials, as with traditional FEM. The DFE technique follows the same typical procedure as FEM by formulating the element equations discretized to a local domain, where element stiffness matrices are constructed and then assembled into a single global matrix.

Analytical methods, such as the Dynamic Stiffness Matrix (DSM), have also been used for the vibrational analysis of isotropic [2, 3], sandwich [5**,** 6**,** 7] and composite structural elements [8] and beam-structure combinations [4, 8]. The DSM approach makes use of the general, closed-form solution to the governing differential equations of motion of the system to formulate a frequency-dependent stiffness matrix. The DSM describes the free vibration of the system and exhibits both inertia and stiffness properties of the system and produces exact results, within the limits of the theory, for simple structural elements, such as uniform beams, using only one element [2, 3]. Banerjee and his colleagues [2- 9] have developed a number of DSM formulations for various beam configurations, where the root-finding technique proposed by Wittrick-Williams (W-W) [53] was exploited to determine the eigenvalues of the system. The DSM has also been used by Wang et al. [51] to simulate a cracked beam. Wang [50] also

investigated the effects of a through-thickness crack on the free vibration modes, aeroelastic flutter and divergence of a composite wing. Borneman et al. [12] presented explicit expressions of a DSM for the coupled composite beams, exhibiting both material and geometric couplings. These expressions were consequently used to develop a cracked DSM formulation, and the free vibration of doubly coupled cracked composite beams was investigated. Given these considerations, the DSM method for a single beam can be modified to accurately model delaminated multi-layer beams.

FEM analysis of 2-dimensional plates and shells including delaminations has also been investigated. These techniques use similar methods as the layerwise beam models [28], which again would require a library of elements for each configuration considered. The effects of different bonding conditions have been examined by altering the behaviour of interlaminar slip [32]. Damage models have also been incorporated into some solutions [18, 54] in order to accurately predict crack and delamination propagation over time. Other work, using spectral elements to model 2-dimensional delaminated plates has been used to model time-variant mechanics, such as Lamb wave reflections [27]. This behaviour, if modeled accurately, can assist in non-destructive testing of components to locate delaminations.

The aim of this work is to present a complete analytical, FEM, DSM and DFE formulation for the free vibration analysis of delaminated two- and three-layer beams, using the free mode delamination model. The delamination of a two-layer beam (single-delamination) is represented by two intact beam segments; one for each of the top and bottom sections of the delamination. Similarly, the delamination of a three-layer beam (double-delamination) is represented by three intact beam segments. The delaminated region is bounded on either side by intact, full-height beams. The beams transverse displacements are assumed to be governed by the Euler-Bernoulli slender beam bending theory. Shear deformation and rotary inertia, commonly associated with Timoshenko beam theory, are neglected. For harmonic oscillations, the governing equations are developed and used as the basis for the model development. Continuities of forces, moments, displacements and slopes at the delamination tips are enforced, leading to solutions of the system. Assembly of element matrices for the element-

based techniques**,** and in all cases the application of boundary conditions results in a characteristic system of equations representing the system. The FEM model will utilize cubic Hermite interpolation functions of approximation to express the flexural displacement functions, i.e., both field variables and weighting functions [10].

In the following, systematic methods will be formulated for the analysis of various configurations using different approaches. First, the single-delamination configuration will be examined, involving a single, through-width delamination at an arbitrary location oriented parallel to the neutral axis of the intact beam. An analytical solution will be presented, following the same approach presented by [14, 16, 35]. Following this, a traditional finite element formulation will be presented, which will take the continuity conditions required at the delamination tips into account. Additionally, two types of dynamic element formulations will be presented – the dynamic stiffness matrix and dynamic finite elements. These methods take into account the frequency-dependency of the solution in their approximations, making them more accurate than traditional FEM for coarser mesh densities [2-9, 19-22]. Following the formulations, a numerical validation will be presented, comparing the results obtained by the presented models with those for equivalent configurations taken from existing literature. Comments will be made on the solution accuracy and efficiency of the presented dynamic solutions, relative to analytical and FEM solutions.

Next, the double-delamination configuration will be presented, involving two through-width delaminations at the same arbitrary lengthwise location, but at different heightwise locations oriented parallel to the neutral axis of the intact beam. An analytical solution will be presented for this configuration, based on [17]. Then, a traditional finite element formulation will be presented, which again will take into account the continuity conditions at the delamination tips. Since the double-delamination configuration contains many beam elements at overlapping lengthwise locations, a 2- and 3-node beam element model was formulated for double-delaminations, in an attempt to reduce the mesh size while retaining solution accuracy. Finally, DSM and DFE formulations will be presented for this configuration, producing frequency-dependent stiffness matrices. Following this, a numerical comparison will again be

made with values obtained from the literature. Comments will be made on the solution accuracy and efficiency, as before, with emphasis on the quality of results and effort required to obtain those results using dynamic element-based methods as compared to analytical and FEM solutions.

To conclude the model presentation, the penultimate chapter will present a verification of the presented theories using commercial FEM software. Beam element modeling techniques will be explored. A comparison will be made with each FEM model, and discrepancies will be explained and analyzed.

Finally, conclusions will be drawn from the previous chapters and remarks will be made on the results obtained from the presented theory and the usefulness of the formulations with respect to expandability to include other effects, such as coupling or non-constant material and geometric parameters. A discussion on work planned for the future will be presented, based on the trends observed during the current model development.

2. Single Delamination

2.1. Analytical Formulation

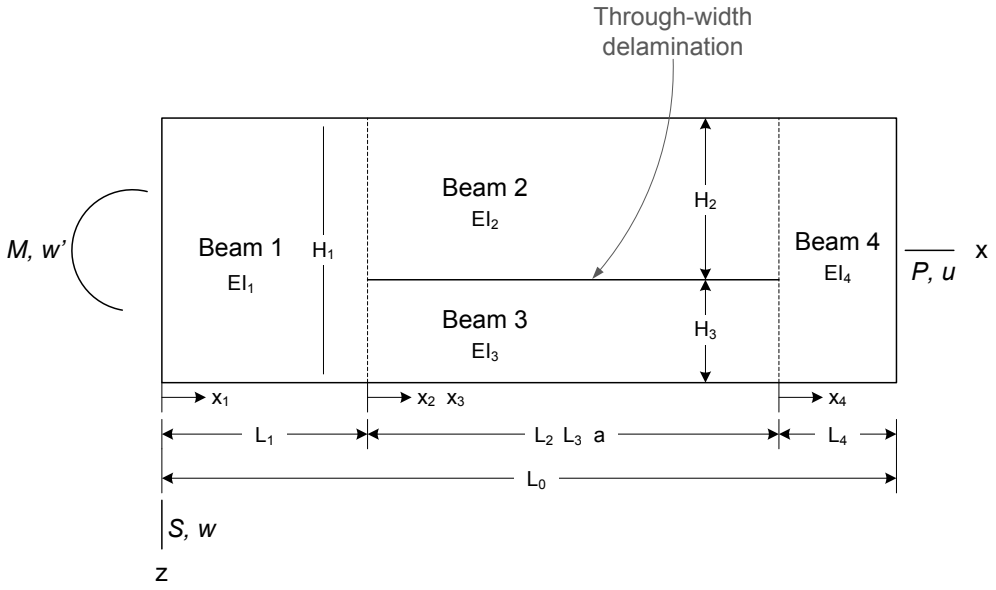

Figure 2 – The co-ordinate system and notation for a single delaminated composite beam

Figure 2 shows the general coordinate system and notation for a delaminated beam, with total length *L*, intact beam segment lengths L_1 and L_4, delamination length *a* and total height H_1. This model incorporates a general delamination, which can include laminated composites or bi-layered isotropic materials, with different material and geometric properties above and below the delamination plane. Thus, the top layer has thickness H_2, Young's modulus E_2, density ρ_2, cross-sectional area A_2 and second moment of area I_2. The bottom layer has corresponding properties, with subscript 3. The delamination tips occur at stations $x_1 = L_1$ and $x_4 = 0$, and torsion, shear deformation, axial (warping effects and axial deformation) and out of plane delamination are ignored. Following this notation, the general equation of motion for the i^{th} Euler-Bernoulli beam in free vibration is written as [14, 17]:

$$EI_i \frac{\partial^4 w_i}{\partial x^4} + \rho_i A_i \frac{\partial^2 w_i}{\partial t^2} = 0\,, \quad i = 1, \ldots 4 \tag{1}$$

For harmonic oscillations, the transverse displacements can be described in the frequency domain by using the transformation

$$w_i(t) = W_i \sin(\omega t) \tag{2}$$

where ω is the circular frequency of excitation of the system, W_i is the amplitude of the displacement w_i, and subscript 'i' represents the beam segment number. By substituting (2) into (1), the equations of motion reduce to

$$EI_i \frac{\partial^4 W_i}{\partial x^4} - \rho_i A_i \omega^2 W_i = 0\,, \;\; i = 1, \ldots 4 \tag{3}$$

The general solution to the 4th-order, homogeneous differential equation (3) can be written in the following form

$$W_i(x_i) = A_i \cos\left(\lambda_i \frac{x_i}{L_i}\right) + B_i \sin\left(\lambda_i \frac{x_i}{L_i}\right) + C_i \cosh\left(\lambda_i \frac{x_i}{L_i}\right) + D_i \sinh\left(\lambda_i \frac{x_i}{L_i}\right) \tag{4}$$

which represents the bending displacement W_i of beam segment 'i', L_i is the beam segment length, and λ_i stands for nondimensional frequency of oscillation, defined as:

$$\lambda_i{}^4 = \frac{\omega^2 \rho_i A_i}{EI_i} L_i^4 \tag{5}$$

Coefficients A_i, B_i, C_i, and D_i (i=1,…4) are evaluated to satisfy the displacement continuity requirements of the beam segments and the system boundary conditions. As also observed and reported by several researchers [14, 17], the inclusion of delamination into the beam model results in a coupling between axial and transverse motion of the delaminated beam segments. This is primarily due to the continuity requirements imposed on the delaminated beam endpoints at the delamination tips. Since the delamination tip cross sections are assumed to remain planar after deformation, the ends of the top and bottom beams must have the same relative axial location after deformation, preventing interlaminar slip. Since the midplanes (assumed to be the neutral axes of the beam segments) in the delaminated segments are located at a distance from the midplanes of the intact segments, they will not have the same axial deformation unless some internal axial force is imposed. This imposed axial will be derived as described by Mujumdar [35].

Consider a delamination tip after deformation. According to the numbering scheme in Figure 2, and since no external axial load is applied, the top and bottom beam segments must have equal and opposite internal axial forces, i.e., $P_3 = -P_2$, applied to prevent interlaminar slip (Figure 3). Additionally, the requirement that the delamination tip faces remain planar after deformation results in, at the left delamination tip:

$$u_2(x_2 = 0) - u_3(x_3 = 0) = \frac{H_1}{2} W_1'(x_1 = L_1) \tag{6}$$

where u_i is the axial displacement of beam section i, and $W_1'(x_1 = L_1) = W_2'(x_2 = 0) = W_3'(x_3 = 0)$ from the kinematic continuity conditions. If this is combined with the same formulation from the right delamination tip,

$$\begin{aligned} &\big(u_3(x_3 = L_3) - u_3(x_3 = 0)\big) - \big(u_2(x_2 = L_2) - u_2(x_2 = 0)\big) \\ &= \frac{H_1}{2}\big(W_4'(x_4 = 0) - W_1'(x_1 = L_1)\big) \end{aligned} \tag{7}$$

The assumption is made by Mujumdar [35] and by other researchers (for example, [14, 17]) that the axial displacement will behave according to the following, for small deformations and material and geometric properties which remain constant along the length of the beam:

$$u_i(x_i = L_i) - u_i(x_i = 0) = \int_0^{L_i} \frac{P_i(x_i)}{EA_i(x_i)} dx_i = \frac{P_i L_i}{EA_i} \tag{8}$$

where EA_i is the axial stiffness of beam section i. Substituting this into (7) yields:

$$\frac{P_2 L_2}{EA_2} - \frac{P_3 L_3}{EA_3} = \frac{H_1}{2}\big(W_4'(x_4 = 0) - W_1'(x_1 = L_1)\big) \tag{9}$$

Using the continuity of axial forces across the delamination tip, $P_3 = -P_2$,

$$P_3 = \Lambda^*\big(W_4'(x_4 = 0) - W_1'(x_1 = L_1)\big) \tag{10}$$

where the parameter Λ^* is defined as

$$\Lambda^* = \frac{H_1}{2L_2}\left(\frac{EA_2EA_3}{EA_2 + EA_3}\right) \tag{11}$$

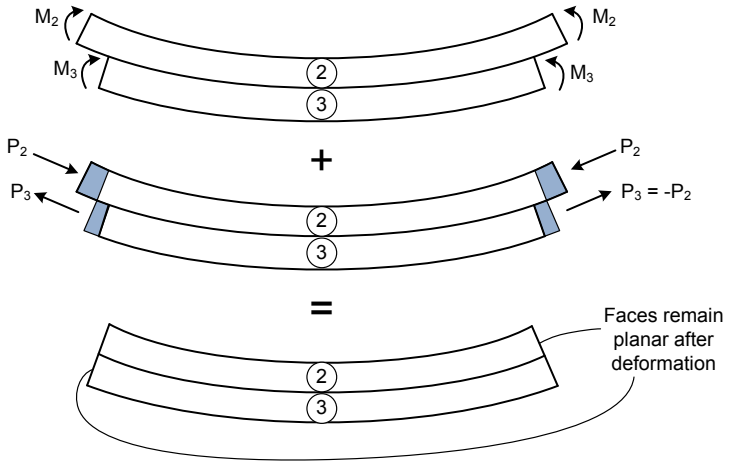

Figure 3 – The faces of the delamination remain planar after deformation (rigid connectors)

At the delamination tips, continuity of bending moments leads to

At the left of delamination tip:
$$M_1(x_1 = \mathrm{L}_1) = M_2(x_2 = 0) + M_3(x_3 = 0) - P_2\frac{H_3}{2} + P_3\frac{H_2}{2} \tag{12}$$

At the right of delamination tip:
$$M_4(x_4 = 0) = M_2(x_2 = \mathrm{L}_2) + M_3(x_3 = \mathrm{L}_3) - P_2\frac{H_3}{2} + P_3\frac{H_2}{2} \tag{13}$$

Using expression (10), which represents the internal axial force, and noting that from beam theory, bending moments and shear forces in beam segment 'i' are related to displacements, W_i, through $M_i = -EI_iW_i''$, and $S_i = EI_iW_i'''$, respectively, it can be shown that, for continuity of bending moments,

$$EI_1W_1''(x_1 = \mathrm{L}_1) = EI_2W_2''(x_2 = 0) + EI_3W_3''(x_3 = 0) + \Lambda[W_4'(x_4 = 0) - W_1'(x_1 = \mathrm{L}_1)] \tag{14}$$

where the coefficient Λ is defined as:

$$\Lambda = \frac{H_1^2}{4L_2}\left(\frac{EA_2EA_3}{EA_2 + EA_3}\right) \tag{15}$$

Likewise, to satisfy the continuity of shear forces about the left delamination tip,

$$EI_1W_1'''(x_1 = \mathrm{L}_1) = EI_2W_2'''(x_2 = 0) + EI_3W_3'''(x_3 = 0) \tag{16}$$

Additionally, there exist 2 kinematic continuity conditions at each delamination tip. Again, about the left delamination tip:

$$\begin{aligned} &\text{Continuity of displacements:} && W_1(x_1 = L_1) = W_2(x_2 = 0) = W_3(x_3 = 0) \\ &\text{Continuity of slopes:} && W_1'(x_1 = L_1) = W_2'(x_2 = 0) = W_3'(x_3 = 0) \end{aligned} \tag{17}$$

These kinematic and force continuity conditions, when applied to each delamination tip, produce six equations per tip. In addition to four endpoint boundary conditions of the system, this process results in 16 equations. If the general solution from (4) is applied to each of the four beam sections, this results in 16 unknown constant coefficients. The 16 equations can be solved simultaneously, using a root finding algorithm to find the natural frequencies and mode shapes of the system. Thus, an analytical solution can be produced for each set of imposed boundary conditions. One of the advantages of utilizing an element-based approach, such as FEM, DSM, or DFE is that the system need not be re-developed for a different set of boundary conditions.

2.2. Finite Element Method (FEM) Formulation

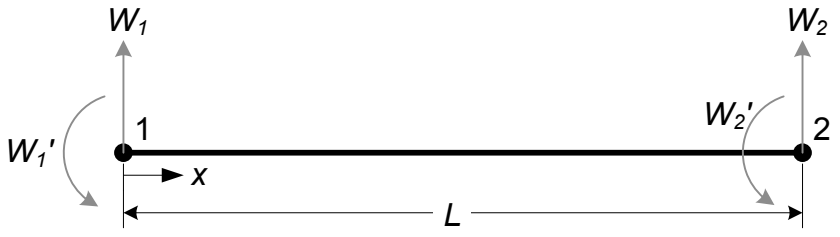

Figure 4 – A 2-node, 4 degree-of-freedom beam element

The finite element approach used here is based on the Galerkin method of weighted residuals. The equations of motion for each beam are used as the basis of this solution method.

Simple harmonic motion is again assumed, and the equations of motion, according to the Euler-Bernoulli beam theory, take the following form:

$$EI_i \frac{\partial^4 \bar{W}_i}{\partial x^4} - EI_i \left(\frac{\lambda_i}{L_i}\right)^4 \bar{W}_i = 0\,, \quad i = 1, \dots 4 \tag{18}$$

where $\bar{W}_i$ is the actual transverse displacement of beam i, and the same non-dimensionalization used in (5) has been applied. An approximate transverse displacement W_i is introduced in place of the actual displacement, such that $W_i \cong \bar{W}_i$. This results in the following residual equation

$$EI_i \frac{\partial^4 W_i}{\partial x^4} - EI_i \left(\frac{\lambda_i}{L_i}\right)^4 W_i = \mathcal{R}\,, \quad i = 1, \dots 4 \tag{19}$$

where $\mathcal{R}$ is the residual of the approximate equation. Following the Galerkin method of weighted residuals, the residual above is weighted by a virtual displacement δW and the integral is set to zero across the domain of the system. Since the system is composed of 4 distinct beam sections occupying their own subset of the domain, the following is representative of the Galerkin method applied to the delaminated system:

$$\sum_{i=1}^{4} \left(\int_0^{L_i} \left(EI_i \delta W_i W_i'''' - EI_i \left(\frac{\lambda_i}{L_i}\right)^4 \delta W_i W_i \right) \mathrm{d}x_i \right) = 0 \tag{20}$$

with $$W_i(x_i) = \langle N_i(x_i) \rangle \{W_n\}$$

where $\langle N_i(x_i) \rangle$ are the shape functions of the beam elements, which will be defined later. Since the virtual displacement is applied to the entire domain, and the four different beam sections occupy unique sub-domains, $\delta W = \sum_{i=1}^{4} \delta W_i$. In order to produce the force and displacement continuity terms, a set of integrations by parts is performed on the above, resulting in the following weak form:

$$\underbrace{\sum_{i=1}^{4} \left(EI_i [\delta W_i W_i''' - \delta W_i' W_i'']_0^{L_i} \right)}_{*} + \sum_{i=1}^{4} \left(\int_0^{L_i} \left(EI_i \delta W_i'' W_i'' - EI_i \left(\frac{\lambda_i}{L_i}\right)^4 \delta W_i W_i \right) \mathrm{d}x_i \right) = 0 \tag{21}$$

The terms in (*), above, represent the boundary and continuity conditions imposed on the system. Using Euler-Bernoulli beam theory, the shear force and bending moment at any point are defined based on the transverse displacement as:

$$\begin{aligned} S(x) &= EI(x)W(x)''' \\ M(x) &= EI(x)W(x)'' \end{aligned} \tag{22}$$

For the endpoints of beam sections 1 and 4, the following is true for free vibration:

$$\begin{aligned} EI_1(\delta W_1 W_1''' - \delta W_1' W_1'')|_{x_1=0} &= \delta \mathcal{W}_{ext}|_{x_1=0} \\ EI_4(\delta W_4 W_4''' - \delta W_4' W_4'')|_{x_4=L_4} &= \delta \mathcal{W}_{ext}|_{x_4=L_4} \end{aligned} \tag{23}$$

where $\delta \mathcal{W}_{ext}$ is the external virtual work caused by applied external forces on the system, causing virtual displacements. For the free vibration of this system, the total external work is $\delta \mathcal{W}_{ext} = \delta \mathcal{W}_{ext}|_{x_1=0} + \delta \mathcal{W}_{ext}|_{x_4=L_4} = 0$. The remaining terms in (*) above can be resolved by applying the continuity conditions from (16) and (17), with the following as a result:

$$\begin{aligned} \sum_{i=1}^{4} \left(EI_i [\delta W_i W_i''' - \delta W_i' W_i'']_0^{L_i} \right) = \delta \mathcal{W}_{ext} \\ + \delta W_2(0) \underbrace{\left(EI_1 W_1'''(L_1) - EI_2 W_2'''(0) - EI_3 W_3'''(0) \right)}_{**} \\ - \delta W_2'(0) \left(EI_1 W_1''(L_1) - EI_2 W_2''(0) - EI_3 W_3''(0) \right) \\ - \delta W_2(L_2) \underbrace{\left(EI_4 W_4'''(0) - EI_2 W_2'''(L_2) - EI_3 W_3'''(L_3) \right)}_{***} \\ + \delta W_2'(L_2) \left(EI_4 W_4''(0) - EI_2 W_2''(L_2) - EI_3 W_3''(L_3) \right) \end{aligned} \tag{24}$$

The terms (**) and (***) in equation (24), as well as the external work term go to zero directly as a result of the shear force continuity conditions. However, the remaining terms do not vanish, since the continuity of bending moments contains an additional implicit bending-axial coupling term, in (14), such that

$$\sum_{i=1}^{4} \left(EI_i [\delta W_i W_i''' - \delta W_i' W_i'']_0^{L_i} \right) = \left(\delta W_2'(L_2) - \delta W_2'(0) \right) \left(\Lambda \left(W_2'(L_2) - \delta W_2'(0) \right) \right) \tag{25}$$

With the boundary and continuity conditions satisfied, the system can be discretized into elements, which will each be approximated using their own basis functions, from which FE shape functions can be found. The system can be discretized as follows, using the result of (25):

$$\Lambda\big(\delta W_2'(L_2) - \delta W_2'(0)\big)\big(W_2'(L_2) - \delta W_2'(0)\big) + \sum_{i=1}^{4} \sum_{m=1}^{\#\, elements_i} \left(\int_{x_m}^{x_{m+1}} \left(EI_i \delta W_i'' W_i'' - EI_i \left(\frac{\lambda_i}{L_i}\right)^4 \delta W_i W_i \right) dx \right) = 0 \tag{26}$$

where '$\#\, elements_i$' is the number of elements in beam section i. Following the traditional Euler-Bernoulli finite element development, Hermite cubic polynomials [33] will be used as the basis functions of approximation for each beam, such that, for a two-node, 2 degree-of-freedom per node beam element (transverse displacement and slope defined at each node)

$$W(x) = \langle 1 \quad x \quad x^2 \quad x^3 \rangle \{C\} \tag{27}$$

where $\{C\}$ is a column vector of unknown constant coefficients. The following represents the vector of nodal displacements used in further FE development:

$$\{W_n\} = \begin{Bmatrix} W_1 \\ W_1' \\ W_2 \\ W_2' \end{Bmatrix} = \begin{bmatrix} 1 & 0 & 0 & 0 \\ 0 & 1 & 0 & 0 \\ 1 & L & L^2 & L^3 \\ 0 & 1 & 2L & 3L^2 \end{bmatrix} \{C\} = [P_n]\{C\} \tag{28}$$

Thus $$W(x) = \langle 1 \quad x \quad x^2 \quad x^3 \rangle [P_n]^{-1} \{W_n\} = \langle \boldsymbol{N}(\boldsymbol{x}) \rangle \{\boldsymbol{W_n}\}$$

$\langle N(x) \rangle$ is a row vector of shape functions, which describe the displacements at any point along the domain of the element in terms of the nodal displacements at the endpoints of the element domain, $\{W_n\}$. Additionally, the shape functions may also be used to approximate the virtual displacements, $\delta W(x) = \langle N(x) \rangle \{\delta W_n\}$. With the shape functions fully defined, they may be substituted for the approximate displacements in (26)

$$\langle \delta W_n \rangle \Big(\Lambda\big(\{N_2\}'(L_2) - \{N_2\}'(0)\big)\big(\langle N_2 \rangle'(L_2) - \langle N_2 \rangle'(0)\big) \Big) \{W_n\} + \sum_{i=1}^{4} \sum_{n=1}^{\#\, elements_i} \langle \delta W_n \rangle \left(\int_{x_m}^{x_{m+1}} \left(EI_i \{N_i\}'' \langle N_i \rangle'' - EI_i \left(\frac{\lambda_i}{L_i}\right)^4 \{N_i\} \langle N_i \rangle \right) dx \right) \{W_n\} = 0 \tag{29}$$

Frequency-dependent and non-frequency-dependent terms above can be gathered to form the following eigenvalue problem, common to structural vibration analysis with FEM, with a modification caused by the presence of the delamination:

$$\langle \delta W_n \rangle \left((\mathbf{K} + \mathbf{K_{delam}}) - \omega^2 \mathbf{M} \right) \{W_n\} = \mathbf{0} \tag{30}$$

if $$\det\left((\mathbf{K} + \mathbf{K_{delam}}) - \omega^2 \mathbf{M} \right) = 0$$

where $\mathbf{K}$ is the structural stiffness matrix formed by assembling the associated beam elements, as per equation (29), $\mathbf{K_{delam}}$ is the delamination stiffness matrix, from the term appearing outside the integral expression in equation (29), and $\mathbf{M}$ is the structural mass matrix. From this formulation, the simplest solution methods involve eigensolutions. However, sweeping the frequency ω until (30) is satisfied is another solution method which will be used extensively for DSM and DFE solutions outlined below, since no simple eigenvalue problem can be derived for those methods as outlined here for FEM.

2.3. Dynamic Stiffness Matrix (DSM) Formulation

Another solution method for describing the free vibration natural frequencies and mode shapes of a delaminated beam system is the method of the Dynamic Stiffness Matrix. Most actively and recently developed by Banerjee [2-8], this method takes advantage of the analytical solution as a basis for an element-based approach. While the DSM technique does not use traditional FEM methods to formulate a solution, the result of the DSM process, nonetheless, is a stiffness matrix, whose entries are frequency-dependent. In the development presented here, a dynamic stiffness matrix formulation will be presented for the central, delaminated beam sections (2 and 3 from Figure 2), including the coupling relationships, which enforce the continuity conditions at the delamination tips. Additionally, a general DSM formulation, in the form of $\boldsymbol{F} = \boldsymbol{K}\,\boldsymbol{u}$ will be presented, which is used to formulate the stiffness matrices for the intact sections (1 and 4 from Figure 2), which is then assembled to the delaminated section using standard element assembly techniques.

The basis of the DSM technique is that the force-displacement relationship can be found in directly from a general solution to the differential equations of motion, after some manipulation of the equations. In the case of uncoupled motion, the equations presented here will not need to be modified, but the specific techniques used for more complex cases, such as intact sandwich beams can be found in [5-7]. Once expressions for the general solutions for the displacements are found in terms of constant coefficients, the beam theory definitions of the forces are used (in the form of displacement-dependent differential equations) to find the nodal force-nodal displacement relationship, in the form of a stiffness matrix. The equations of motion take the following form, as established previously:

$$EI_i \frac{\partial^4 W_i}{\partial x^4} - EI_i \left(\frac{\lambda_i}{L_i}\right)^4 W_i = 0\,, \quad i = 1, \dots 4 \tag{31}$$

where W_i is now taken to be the actual displacement of the i^{th} beam section, as a function of the axial degree of freedom x_i. The general solution to this equation, in terms of constant coefficients is:

$$W_i(x_i) = A_i \cos\left(\lambda_i \frac{x_i}{L_i}\right) + B_i \sin\left(\lambda_i \frac{x_i}{L_i}\right) + C_i \cosh\left(\lambda_i \frac{x_i}{L_i}\right) + D_i \sinh\left(\lambda_i \frac{x_i}{L_i}\right) \tag{32}$$

Then, the Euler-Bernoulli beam theory equations for the shear force and bending moment are used to describe the internal forces and moments at any point in the domain:

$$\begin{aligned} S_i(x_i) &= EI(x_i)W(x_i)''' \\ M_i(x_i) &= EI(x_i)W(x_i)'' \end{aligned} \tag{33}$$

where $(\cdot)' = \frac{\mathrm{d}(\cdot)}{\mathrm{d}x_i}$. Naturally, the expression (32) can be substituted into (33), since the derivatives of (32) can easily be expressed in terms of the coefficients A_i — D_i. Then, the nodal values of the shear force can be expressed in terms of the coefficients:

$$\boldsymbol{F_i} = \boldsymbol{B_i a_i}, \text{ where } \boldsymbol{a_i} = \langle A_i \quad B_i \quad C_i \quad D_i \rangle^T \tag{34}$$

Furthermore from equation (32), the end displacements and slopes can be related to coefficient vector, $\boldsymbol{a_i}$, through the following expression

$$\boldsymbol{u_i} = \boldsymbol{D_i a_i} \tag{35}$$

where $$\boldsymbol{u_i} = \langle W_i(x_i = 0) \quad W_i'(x_i = 0) \quad W_i(x_i = L_i) \quad W_i'(x_i = L_i)\rangle^T$$

Finally, using expressions (34) and (35), leads to

$$\boldsymbol{F_i} = \boldsymbol{B_i D_i^{-1} u_i} \; = \; \boldsymbol{K_{DSM,i}\, u_i} \tag{36}$$

where $\boldsymbol{K_{DSM,i}}$ is the frequency-dependent, dynamic stiffness matrix of beam section i. The standard assembly process similar to FEM leads to the nonlinear eigenvalue problem of the system:

$$[\overline{K}(\omega)]\{\overline{U}\} = \{0\} \tag{37}$$

where $[\overline{K}(\omega)]$ is the overall (global) dynamic stiffness matrix and $\{\overline{U}\}$ represents the vector of defrees of freedom of the system. The solution of the problem consists of finding the eigenvalue, ω, and corresponding eigenvector, $\{\overline{U}\}$, that satisfy equation (37) and the boundary conditions imposed using, for example, the penalty method [10]. Powerful algorithms exist for solving a linear eigenvalue problem (i.e., system's natural frequencies), resulting from discrete or lumped mass models. In the case of the nonlinear eigenproblem shown in equation (37), which involves frequency-dependent dynamic stiffness matrices arising from the DFE or DSM formulations, one can use the Wittrick-Williams (W-W) root-finding technique [53] to determine the eigenvalues of the system. The W-W algorithm is a simple method of calculating the number of natural frequencies of a system that are below a given trial frequency value. The method exploits the bisection method and the Sturm sequence properties of the dynamic stiffness matrix to converge on any particular natural frequency of the system, to any desired accuracy. This allows one to solve for any specific frequency number without having to solve for all previous frequencies, which is the requirement of some linear eigenvalue solvers. Consequently, the corresponding modes can be evaluated [2-8, 19].

Through continuity conditions, a coupling relationship can be found within the delamination region to reduce the total number of unknowns from eight (A_i — D_i, i =2,3, for the top and bottom beams within the delaminated region) to four. Of particular interest are the continuity conditions for displacement and slope at the delamination tips, from which a coupling between the coefficients for the top beam and the bottom one can be derived. Stemming from the requirement that the displacement and slope of each beam, at the delamination tips, must be equal, the transverse displacements of beam segments 2 and 3 can be linked through the following relationship:

$$\begin{bmatrix} 1 & 0 & 1 & 0 \\ 0 & \frac{\lambda_2}{L_2} & 0 & \frac{\lambda_2}{L_2} \\ \cos(\lambda_2) & \sin(\lambda_2) & \cosh(\lambda_2) & \sinh(\lambda_2) \\ -\frac{\lambda_2}{L_2}\sin(\lambda_2) & \frac{\lambda_2}{L_2}\cos(\lambda_2) & \frac{\lambda_2}{L_2}\sinh(\lambda_2) & \frac{\lambda_2}{L_2}\cosh(\lambda_2) \end{bmatrix} \begin{Bmatrix} A_2 \\ B_2 \\ C_2 \\ D_2 \end{Bmatrix} = \begin{bmatrix} 1 & 0 & 1 & 0 \\ 0 & \frac{\lambda_3}{L_3} & 0 & \frac{\lambda_3}{L_3} \\ \cos(\lambda_3) & \sin(\lambda_3) & \cosh(\lambda_3) & \sinh(\lambda_3) \\ -\frac{\lambda_3}{L_3}\sin(\lambda_3) & \frac{\lambda_3}{L_3}\cos(\lambda_3) & \frac{\lambda_3}{L_3}\sinh(\lambda_3) & \frac{\lambda_3}{L_3}\cosh(\lambda_3) \end{bmatrix} \begin{Bmatrix} A_3 \\ B_3 \\ C_3 \\ D_3 \end{Bmatrix} \tag{38}$$

or $$\boldsymbol{D_2 a_2 = D_3 a_3}$$

Using this result, a direct relationship between the coefficients of beam 2 and 3 can be found. Due to this, the force-displacement relationships of the central delaminated section (2 and 3 from Figure 2) can be expressed in terms of a single set of nodal displacements. This was expected, since it is explicitly required by the kinematic delamination conditions. The result is the following, if for the sake of formulation, $\boldsymbol{u_2}$ is taken to be the reference displacements, even though $\boldsymbol{u_2 = u_3}$:

$$\begin{aligned} \boldsymbol{F_{2,3}} &= \boldsymbol{B_2 a_2 + B_3 a_3} \\ &= \left(\boldsymbol{B_2 + B_3 D_3^{-1} D_2}\right)\boldsymbol{a_2} \\ &= \underbrace{\left(\boldsymbol{B_2 + B_3 D_3^{-1} D_2}\right)\boldsymbol{D_2^{-1}}}_{\boldsymbol{K_{DSM}}}\boldsymbol{u_2} \end{aligned} \tag{39}$$

The final result being a dynamic stiffness matrix, which incorporates the effects of both beams 2 and 3, with one set of nodal displacements, which can be assembled to the intact sections' stiffness matrices, found using (36).

2.4. Dynamic Finite Element (DFE) Formulation

Dynamic Finite Elements (DFE) takes advantage of the accuracy offered to DSM solutions from the frequency-dependent nature of the approximations, with the added benefits that a Galerkin finite element formulation provides. These include the ease of boundary condition modification, coupled material response implementation, non-linear material properties, and more. Using the already discretized weak form equation from the FEM formulation,

$$\Lambda\left(\delta W_2'(L_2) - \delta W_2{}'(0)\right)\left(W_2'(L_2) - \delta W_2{}'(0)\right) + \sum_{i=1}^{4}\sum_{m=1}^{\#\,elements_i}\left(\int_{x_m}^{x_{m+1}}\left(EI_i\delta W_i{}''W_i'' - EI_i\left(\frac{\lambda_i}{L_i}\right)^4\delta W_i W_i\right)dx\right) = 0 \tag{40}$$

another set of integrations by parts is performed on the system. This results in the following, where the differentiation of δW_i and W_i have been reversed from their original form in (20),

$$\begin{aligned}\Lambda\left(\delta W_2'(L_2) - \delta W_2{}'(0)\right)\left(W_2'(L_2) - \delta W_2{}'(0)\right) &+ \sum_{i=1}^{4}\sum_{m=1}^{\#\,elements_i}\left(EI_i[\delta W_i{}''W_i' - \delta W_i{}'''W_i]_{x_m}^{x_{m+1}}\right. \\ &\left. + \int_{x_m}^{x_{m+1}}\left(\underbrace{EI_i\delta W_i{}''''W_i - EI_i\left(\frac{\lambda_i}{L_i}\right)^4\delta W_i W_i}_{*}\right)dx\right) = 0\end{aligned} \tag{41}$$

From this point, unlike traditional finite elements, the basis functions are chosen such that (*) in (41) goes to zero, resulting in the elimination of integral equations for this uncoupled, linear system. The general solution to (*), which will be used as DFE basis functions, is

$$W_i(\xi_i) = \left\langle \cos(\alpha_i\xi_i) \quad \frac{\sin(\alpha_i\xi_i)}{\alpha_i} \quad \frac{\cosh(\alpha_i\xi_i) - \cos(\alpha_i\xi_i)}{{\alpha_i}^2} \quad \frac{\sinh(\alpha_i\xi_i) - \sin(\alpha_i\xi_i)}{{\alpha_i}^3} \right\rangle \{C_i\} \tag{42}$$
$$= \langle \boldsymbol{P_i} \rangle \{\boldsymbol{C_i}\}$$

where $\{C_i\}$ is a column vector of constant coefficients, ξ_i is the non-dimensional axial coordinate, x_i/L_i , and α_i is a constant coefficient from the general solution to (*) in (41), equal to

$$\alpha_i = \frac{\omega^2 \rho_i A_i}{E I_i} \tag{43}$$

The shape functions are a linear combination of the more simplified form introduced in (4), but the specific format of the basis functions serves an important purpose. If the frequency of excitation ω goes to zero, the basis functions here will simultaneously become mathematically identical to the Hermite cubic basis functions, and similarly with the shape functions. If this approach is not taken, then the shape functions diverge as the frequency approaches zero, and the method would not be complete, as static deformation would not be possible to find. The shape functions were found using the following,

$$\{W_n\} = \begin{Bmatrix} W_i(\xi_i = 0) \\ W_i'(\xi_i = 0) \\ W_i(\xi_i = 1) \\ W_i'(\xi_i = 1) \end{Bmatrix} = \begin{bmatrix} 1 & 0 & 0 & 0 \\ 0 & 1 & 0 & 0 \\ \cos(\alpha_i) & \frac{\sin(\alpha_i)}{\alpha_i} & \frac{\cosh(\alpha_i) - \cos(\alpha_i)}{{\alpha_i}^2} & \frac{\sinh(\alpha_i) - \sin(\alpha_i)}{{\alpha_i}^3} \\ -\alpha sin(\alpha_i) & \cos(\alpha_i) & \frac{\alpha\sinh(\alpha_i) + \alpha\sin(\alpha_i)}{{\alpha_i}^2} & \frac{\alpha\sinh(\alpha_i) - \alpha\cos(\alpha_i)}{{\alpha_i}^3} \end{bmatrix} \tag{44}$$
$$= [\boldsymbol{P_n}]_i \{\boldsymbol{C_i}\}$$

Thus
$$W_i(\xi_i) = \langle P \rangle [P_n]_i^{-1} \{W_n\} = \langle \boldsymbol{N_i} \rangle \{\boldsymbol{W_n}\} \tag{45}$$

where $(\cdot)_n$ represents the nodal values at the endpoints of the beam element. It should be noted also that, while the coordinate non-dimensionalization to ξ_i was made, the differentiation is still with respect to x_i , and this should be respected in the formulation.

2.5. Numerical Tests

Numerical checks were performed to confirm the predictability, accuracy and practical applicability of the proposed DSM method. To solve the nonlinear eigenproblem (37) resulting

from DSM formulation, a determinant search method was used; the non-dimensional frequency was swept, searching a particular frequency, ω, which would make the determinant of the global dynamic stiffness matrix zero, $|\overline{K}(\omega)| = 0$, whose corresponding eigenvector, $\{\overline{U}\}$, represented the degrees of freedom of the mode shape associated with the natural frequency. The use of the non-dimensional frequency (5) in the calculations removed material dependencies from the system, provided that the material was isotropic, or at least orthotropic with principal axes aligned with the Cartesian coordinate system in Figure 1.

In what follows, an illustrative example of fixed-fixed, homogeneous, 2-layer delaminated beam will be examined. The natural frequencies of the system with a central split, about the mid-section ($L_1 = L_4$), of various lengths up to 60% of the span ($0 \leq a/L \leq 0.6$), occurring symmetrically along the midplane of the beam and surrounded by intact beam segments, are considered. This split beam configuration has also been presented and studied in [14, 35, 49]. The FEM, DSM, and DFE models were created and used to compute the natural frequencies and mode shapes of various delamination cases. As the benchmarks for comparison, the results from references [14, 35, 49] as well as an alternative formulation from [28] were used to validate the solution methods. Also as suggested in [49], the first two frequencies were computed for a delamination length of $0.0002L$, to check for numerical instability when the split length becomes extremely small. This case showed negligible discrepancies from those of a solid intact beam.

A split beam FEM model was formulated, exploiting cubic Hermite [10] interpolation functions. Using the model presented in Section 2.2, the weigted residual method was applied on the differential equations governing the free vibration of 2-layer delaminated beams. The residual was made orthogonal to a virtual displacement over the domain of the element, and two integrations by parts were carried out to reduce the continuity requirements of displacement functions. The principle of virtual work was used to determine the element system equations. As presented earlier, the differential stretching of the top and bottom layers was present to keep the delamination faces planar after deformation (i.e., no interlaminar slip at the delamination faces). The FEM formulation results in an additional stiffness term not

present if interlaminar slip were included. This 'delamination stiffness' has the effect of stiffening the system at the delamination tips. Table 1 summarizes the first two natural frequencies obtained using the developed (cubic Hermite-type) finite element model (FEM), with 6- and 10-element discretizations of midplane delaminated region (60% of span). The intact beam segments were modeled using single beam elements. As can be seen from Table 1, the FEM frequencies exhibit a convergence towards the DSM results, as the number of elements is increased. Conventional FEM natural frequencies reported by Lee (2000) [28] are also presented for reference.

Table 1 – Natural frequency parameter λ^2 of a single delaminated beam. FEM sensitivity presented

Delam. Length a/L_{tot}	Wang et al. [49]		Analytical		FEM†; 6 Elements		FEM†; 10 Elements		Layerwise FEM [28]	
	Mode 1	Mode 2	Mode 1	Mode 2	Mode 1	Mode 2	Mode 1	Mode 2	Mode 1	Mode 2
Intact	22.39	61.67	22.39	61.67	-	-	-	-	22.36	61.61
0.1	22.37	60.76	22.37	60.76	22.37	60.77	22.37	60.76	22.36	60.74
0.2	22.35	55.97	22.36	55.99	22.36	56.01	22.36	55.99	22.35	55.95
0.3	22.23	49.00	22.24	49.03	22.24	49.05	22.24	49.03	22.23	48.97
0.4	21.83	43.87	21.84	43.90	21.84	43.95	21.84	43.90	21.82	43.86
0.5	20.88	41.45	20.89	41.52	20.89	41.57	20.89	41.55	20.88	41.50
0.6	19.29	40.93	19.30	41.03	19.29	41.08	19.29	41.04	19.28	41.01

† Conventional FEM displays numerical instabilities with delamination lengths approaching 0

The FEM formulation produced excellent agreement with both the analytical results (including from the literature) as well as with the layerwise FEM theory. It can be seen that the FEM result discrepancy was low, even for a coarse mesh size. It was observed that the discrepancy for the first natural modes was lower than for the second natural modes. This is consistent with traditional FEM theory, where more elements are required to guarantee accurate solutions for higher mode numbers.

Table 2 summarizes the DSM results for the first two natural frequencies of the system. The DSM results are compared to those presented by Wang et al. [49] and Della and Shu [17]. The DSM model incorporates a total of only three ‘elements’; one intact element on each end of the delamination representing the undamaged beam segments (1 and 4), obtained using the methods outlined in previous sections, and one fully delaminated element.

Table 2 – Natural frequency parameter λ^2 of a single delaminated beam. DSM, CM, and FEM [28] models

Delamination Length a/L_{tot}	Wang, et al. [49]		DSM		Della and Shu [17]		Layerwise FEM [28]	
	Mode 1	Mode 2	Mode 1	Mode 2	Mode 1	Mode 2	Mode 1	Mode 2
Intact	22.39	61.67	22.39	61.67	22.37	61.67	22.36	61.61
0.1	22.37	60.76	22.37	60.80	22.37	60.76	22.36	60.74
0.2	22.35	55.97	22.36	55.99	22.36	55.97	22.35	55.95
0.3	22.23	49.00	22.24	49.00	22.24	49.00	22.23	48.97
0.4	21.83	43.87	21.83	43.89	21.83	43.87	21.82	43.86
0.5	20.88	41.45	20.89	41.52	20.89	41.45	20.88	41.50
0.6	19.29	40.93	19.30	41.03	19.30	40.93	19.28	41.01

The DSM natural frequencies are in excellent agreement with those reported in the literature, with a maximum difference of 0.24%. It is also worth noting that a slight dissimilarity was found between the 2nd natural frequency values (61.67, 60.76, 55.97, 49.00, 43.87, 41.45, and 40.93, respectively) reported in Table 1 of reference [49] and the same data reported in [17]. Conventional FEM natural frequencies obtained based on layerwise theory, as reported by Lee (2000) [28], are also presented for comparison. Excellent agreement was found between the DSM and these FEM results.

Additionally, the presented DFE solution was used to compute the natural frequencies and mode shapes of selected delamination cases. A clamped-clamped beam with a central delamination (L_1=L_4) surrounded by intact beam segments, was modeled again. FEM and DSM were used to compare the results.

In order to solve for the natural frequencies of the system, a sweep of the non-dimensional frequency was performed, and a search for the following condition was carried out, which represents free vibration of the assembled system:

$$[K(\omega)]\{w_n\} = 0 \quad \text{if} \quad |K(\omega)| = 0$$

where the assembly of local element stiffness matrices was carried out in the traditional FEM manner. The use of the non-dimensional frequency λ^2 removed material dependencies from

the system, provided that the material was isotropic, or at least orthotropic with principal axes aligned with the Cartesian coordinate system in Figure 2.

Table **3** summarizes the DFE results, comparing them with DSM and Wang, et al. [49] for the free mode delamination model. The initial results, even for 4 elements, agree well with those results taken from the literature. This provides promise for using the DFE technique as a possible Mesh Reduction Method (MRM) in the analysis of delaminated beams, as it has been used previously for undamaged beams [19-22].

Table 3 – Natural frequency parameter λ^2 of a single-delaminated beam. DSM, DFE presented

Delamination Length a/L_0	Wang, et al. [49]		DSM		DFE 4 Elements†		DFE 8 Elements†	
	Mode 1	Mode 2	Mode 1	Mode 2	Mode 1	Mode 2	Mode 1	Mode 2
intact	-	-	22.39	61.67	22.39	61.67	22.39	61.67
0.1	22.37	60.76	22.37	60.80	22.37	60.81	22.37	60.80
0.2	22.35	55.97	22.36	55.99	22.36	56.00	22.36	55.99
0.3	22.23	49.00	22.24	49.00	22.24	49.00	22.24	49.00
0.4	21.83	43.87	21.83	43.89	21.84	43.90	21.83	43.89
0.5	20.88	41.45	20.89	41.52	20.89	41.52	20.89	41.52
0.6	19.29	40.93	19.30	41.03	19.29	41.03	19.30	41.03

† - 4 and 8 element meshing contains a single element and 2 elements, respectively per beam section in Figure 2.

From the results presented above, it is clear that even a single DFE element per beam section produced excellent agreement with the DSM formulation and with those results obtained from existing literature. In particular, the agreement observed between a coarse-mesh DFE model and analytical solutions for higher modes is of note. Using traditional FEM-based solution methods, higher mode information requires the use of a finer mesh. The number of elements required for a mode number for good accuracy scales with the mode number, as the natural frequencies and mode shape information are dependent on the size of the mass and stiffness matrices and thus, the number of nodes present in the mesh. DFE does not exhibit this dependency, and in theory, an infinite number of modes can be found using the smallest mesh possible, provided that for very high frequencies, the root-finding algorithm does not suffer from numerical overflow. To illustrate this point, traditional FEM-based solutions

were obtained using the FEM formulation presented earlier, with the following results for a centrally-located through-width delamination:

Table 4 – Natural frequency parameter λ^2 of a single-delaminated beam. DFE, FEM presented

Delamination Length a/L_0	DFE 4 Elements†		FEM 8 Elements††		FEM 20 Elements††	
	Mode 1	Mode 2	Mode 1	Mode 2	Mode 1	Mode 2
intact	22.39	61.67	-	-	-	-
0.1	22.37	60.81	22.54	69.37	22.37	60.60
0.2	22.36	56.00	22.42	58.56	22.36	56.05
0.3	22.24	49.00	22.27	49.63	22.24	49.57
0.4	21.84	43.90	21.87	44.24	21.84	44.01
0.5	20.89	41.52	20.97	42.20	20.89	41.55
0.6	19.29	41.03	19.44	42.77	19.29	41.04

† - 4 and 8 element meshing contains a single element and 2 elements, respectively per beam section in Figure 2.
†† - 8 and 20 element meshing contains 2 elements and 5 elements, respectively per beam section in Figure 2.
Conventional FEM displayed numerical instability for delamination lengths approaching 0

While the first mode shows fair agreement between DFE and FEM for the coarse FEM mesh, the second exhibited a maximum discrepancy of 12%. In contrast, when the number of elements was increased, the FEM formulation exhibited much better correlation with the DFE results, and by extension from Table 4, with analytical results as well. This trend of increasing FEM accuracy with finer mesh density was expected, but also served to highlight the utility of a dynamic formulation such as DFE for obtaining information about higher natural modes.

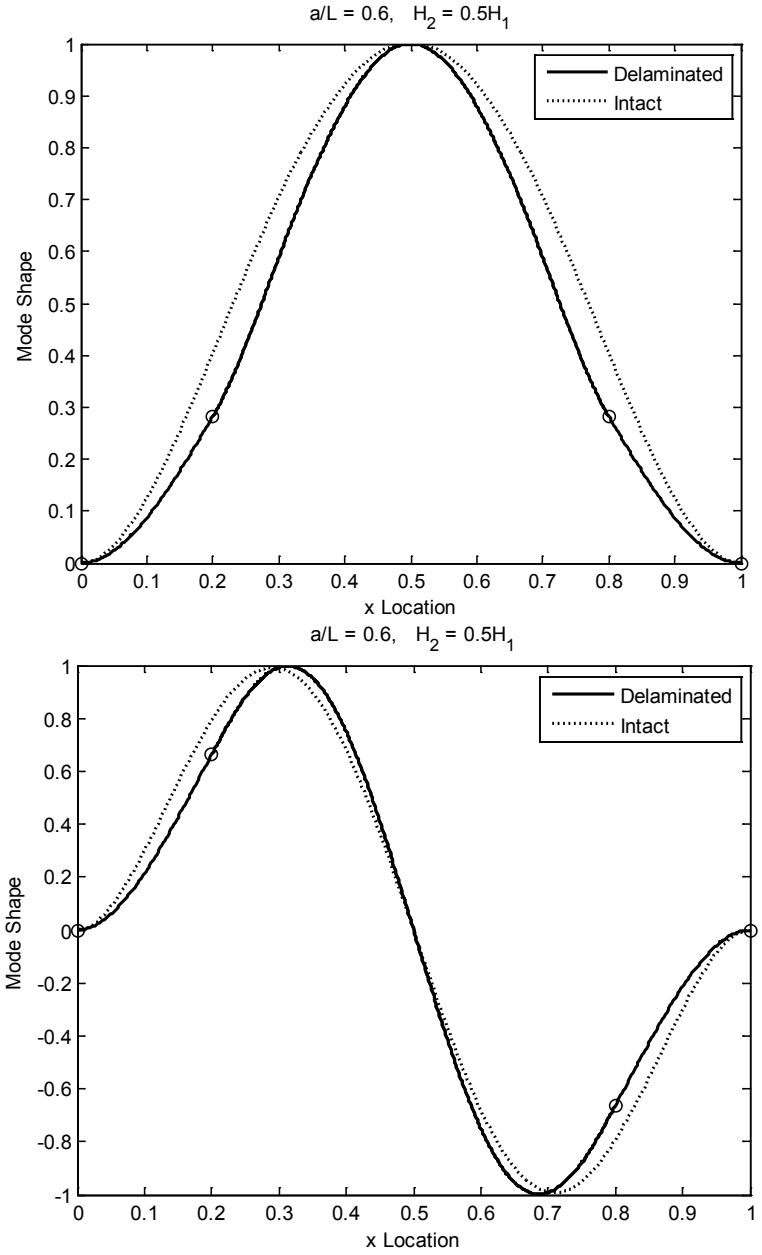

Figure 5 – The first two natural modes of a single-delaminated beam. Top: First mode shape; Bottom: Second mode shape. Intact mode shapes are also visualized.

Figure 5 shows the first two natural modes of the 2-layered beam, with 60% of span midplane delamination, compared with those of an intact configuration. It is worth noting that the conventional FEM-based models are characterized by constant mass and stiffness matrices, in the frequency domain, of limited number of total degrees of freedom (DOF); i.e., number of nodes times number of DOF per node. Accordingly, the natural modes obtained from the

conventional FEM model – being the eigenmodes of the governing linear eigenvalue problem – have the same dimension as the total degrees of freedom of the FEM model. Unlike the conventional FEM (e.g., 4-DOF Hermite beam element), the DSM and frequency-dependent DFE matrices are formulated based on continuous element assumptions, which introduces infinite number of degrees of freedom within each element (see, e.g., [2-9, 46, 52]). Therefore, through the use of these techniques, additional modes of vibration can be found than would otherwise be available using FEM with an equal number of elements. Additionally, certain modes of vibration are the result of the denominator of the global dynamic stiffness matrix going to zero; and correspondingly the determinant of the global stiffness matrix approaching infinity, $|\overline{K}(\omega)| \to \infty$. Also known as the poles of a system, they can represent real physical mode shapes [51, 52] even though at least one eigenvalue goes to zero. Through simplification, it was found that the denominator of the dynamic stiffness matrix (DSM and DFE), has the following form:

$$DEN = \cos(\lambda_2)\cosh(\lambda_2) - 1$$

While the mode shapes of the poles were not necessarily important in this analysis, their corresponding natural frequencies are important when using more advanced root solving techniques [51, 52]. Zero-nodal-displacement modes have also been observed and reported in the literature for other structural configurations (see, for example, [46, 51, 52]). There are also certain frequencies captured through the modal analysis whose mode shapes, while mathematically possible, do not represent physically admissible displacements. These modes – for example a natural mode at λ^2 = 31.0 in the case of present study – are simply the result of the free model assumptions [35]. They correspond to interpenetration of the beams and would not be present in a constrained mode analysis. As seen in Figure 6, the vibration of the top and bottom delaminated beams would be inadmissible due to non-linear phenomena such as contact, which cannot be modeled in the frequency domain. Similar inadmissible partial and complete interpenetration modes have also been reported in the literature [39].

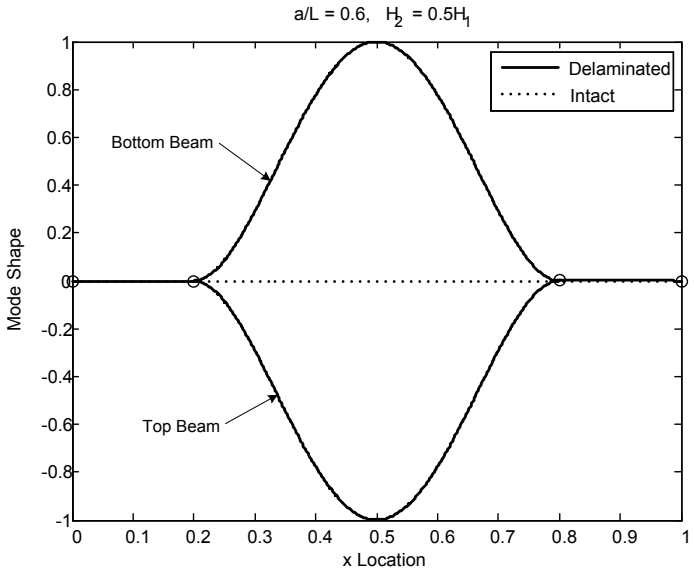

Figure 6 – The first opening mode shape for a midplane delamination. $\lambda^2 = 31.88$

In addition to real natural modes of vibration, poles and inadmissible interpenetration modes examined above, under small vibration amplitudes a split layered beam may exhibit a mode at a frequency corresponding to a delamination-opening mode. Figure 5 shows the first opening mode for a delaminated beam with top beam thickness equal to 40% the height of the intact beam, 60% of span, off-midplane delamination, obtained using DSM, DFE and FEM models (FEM nodes visualized). Similar opening modes have also been reported in the literature (see, e.g. [14, 17]).

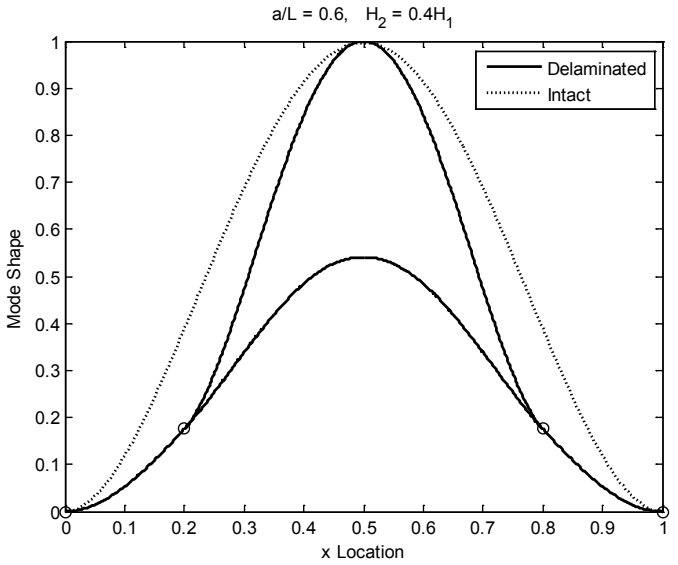

Figure 7 – The first mode shape for an off-midplane delamination. $\lambda^2 = 36.88$

3. Double Delamination

3.1. Analytical Formulation

The study of delaminated composite beams is not limited to a single through-width delamination. In fact, the literature contains many examples of different delamination configurations. To show the extensibility of the dynamic modelling presented in the previous section, a multiple-delaminated beam model will be analyzed and the results compared to analytical formulations, as well as data obtained from the literature.

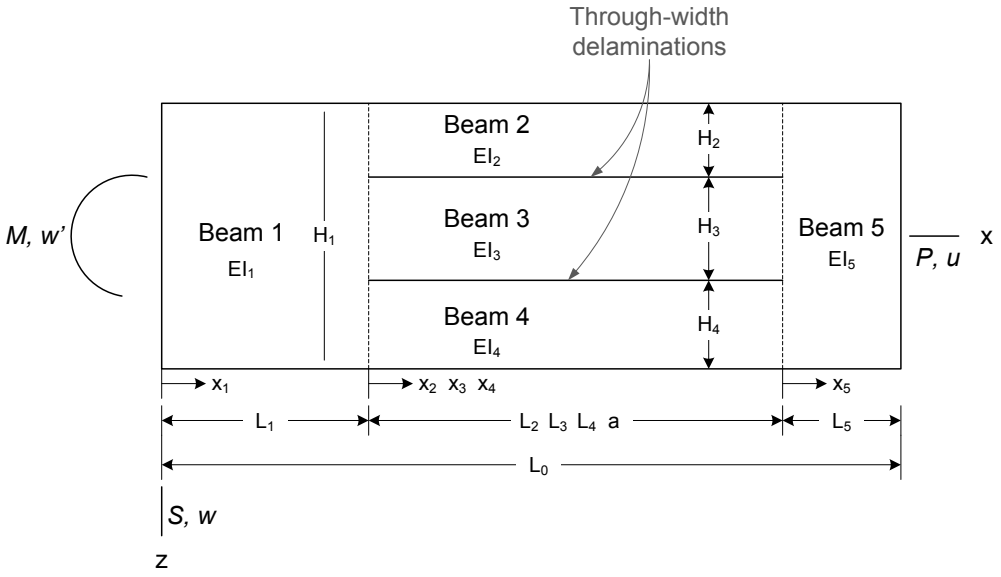

Figure 8– The co-ordinate system and notation for a double delaminated composite beam

According to Euler-Bernoulli beam theory, each beam section will deform according to the differential equation of motion

$$EI_i \frac{\partial^4 w_i}{\partial x^4} + \rho_i A_i \frac{\partial^2 w_i}{\partial t^2} = 0\,, \quad i = 1, \dots 5 \tag{46}$$

For harmonic oscillations, the transverse displacements can be described in the frequency domain by using the transformation

$$w_i(t) = W_i \sin(\omega t) \tag{47}$$

where ω is the circular frequency of excitation of the system, W_i is the amplitude of the displacement w_i, and subscript 'i' represents the beam segment number. By substituting (47) into (46), the equations of motion reduce to

$$EI_i \frac{\partial^4 W_i}{\partial x^4} - \rho_i A_i \omega^2 W_i = 0\,, \quad i = 1, \ldots 5 \tag{48}$$

The general solution to the 4th-order, homogeneous differential equation can be written in the following form

$$W_i(x_i) = A_i \cos\left(\lambda_i \frac{x_i}{L_i}\right) + B_i \sin\left(\lambda_i \frac{x_i}{L_i}\right) + C_i \cosh\left(\lambda_i \frac{x_i}{L_i}\right) + D_i \sinh\left(\lambda_i \frac{x_i}{L_i}\right) \tag{49}$$

which represents the bending displacement W_i of beam segment 'i', L_i is the beam segment length, and λ_i represents the nondimensional frequency of oscillation, defined as:

$$\lambda_i{}^4 = \frac{\omega^2 \rho_i A_i}{EI_i} L_i^4 \tag{50}$$

The expressions (46) through (50) are, respectively, identical to (1) through (5) presented in Chapter 2. The basic assumption at the delamination tips, again, is that the change in length of the delaminated beams, as imposed by requirement that the delamination tips remain planar after deformation (rigid connectors), is equal to the length change caused by an internal axial force acting at the delaminated beam endpoints (see Figure 1). In this way, the axial forces can be treated as unknown and solved to provide sufficient information to generate bending moment continuity equations at the delamination tips. These moment continuity equations include the following factors, for equal-length double delaminations, written about the left delamination tip:

$$\begin{aligned} M_1 = EI_1 W_1'' = {} & EI_2 W_2'' + EI_3 W_3'' + EI_4 W_4'' \\ & + \boldsymbol{P_2 \frac{H_2}{2} + P_3 \left(H_2 + \frac{H_3}{2}\right) + P_4 \left(H_2 + H_3 + \frac{H_4}{2}\right)} \end{aligned} \tag{51}$$

The terms in bold (the last three terms in equation (51)) represent the moment contribution from the axial forces, which are unknown at this point and are treated as variable.

In order to find the values of these axial forces as functions of the displacement magnitude, W – which when solved will be an appropriate approximation function – some physical assumptions have to be made. Equilibrium of axial forces at either delamination tips demands that $P_2+P_3+P_4=0$, assuming the system has no externally applied axial forces. Additionally, the following conditions, based on the assumption that the differential axial stretching is caused completely by the unknown axial forces, can be written:

$$\begin{aligned}\frac{P_2 a}{EA_2}-\frac{P_3 a}{EA_3}&=\left(W_5'(x_5=0)-W_1'(x_1=L_1)\right)\frac{H_2+H_3}{2}\\ \frac{P_3 a}{EA_2}-\frac{P_4 a}{EA_3}&=\left(W_5'(x_5=0)-W_1{}'(x_1=L_1)\right)\frac{H_3+H_4}{2}\end{aligned} \tag{52}$$

where the terms on the right represent the differential stretching to maintain axial displacement continuity at the delamination tips and the terms on the left represent the stretching/shrinking caused by the axial forces. This is the same technique used in Chapter Analytical Formulation2.1 to find the equivalent statement for the single delamination case. Setting these two equal, the form of the axial forces can be determined as functions of the difference in slope between the delamination tips, $W_1'(x_1=L_1)-W_5'(x_5=0)$. The moment continuity equation above then becomes, after substitution and simplification:

$$EI_1W_1''=EI_2W_2''+EI_3W_3''+EI_4W_4''+\Lambda\left(W_1'(x_1=L_1)-W_5'(x_5=0)\right)$$

where $$\Lambda=\frac{(H_1+H_3)^2EA_2EA_4+(H_2+H_3)^2EA_2EA_3+(H_3+H_4)^2EA_3EA_4}{4a(EA_2+EA_3+EA_4)} \tag{53}$$

Similarly, the form of the moment continuity condition at the right delamination tip can be found. In addition, the other continuity conditions at the delamination tips may be found. For example at the left delamination tip:

$$\begin{aligned}&\text{Continuity of displacements:} && W_1=W_2=W_3=W_4\\ &\text{Continuity of slopes:} && W_1{}'=W_2{}'=W_3{}'=W_4{}'\\ &\text{Continuity of shear forces:} && EI_1W_1'''=EI_2W_2'''+EI_3W_3'''+EI_4W_4'''\end{aligned} \tag{54}$$

Using the requirement for a force-displacement relationship with the already established general solution, the standard, Euler-Bernoulli beam theory descriptions of internally developed bending moment and shear stress may be written at each point x_i as:

$$M_i = EI_i \frac{d^2 W_i(x_i)}{dx_i{}^2}$$
$$S_i = EI_i \frac{d^3 W_i(x_i)}{dx_i{}^3} \tag{55}$$

Similar relationships can be derived for the right delamination tip. These relationships result in 20 equations, and 20 unknown constants, from the $\{C_i\}$ vectors. When the determinant of the coefficient matrix of these constants vanishes, the conditions for natural modes of free vibration are met, and the frequencies at which this occurs are the natural frequencies of the system. These frequencies may be found in a number of ways, from a frequency-sweep to more advanced root-finding algorithms [53].

3.2. Finite Element Method (FEM) Formulation

The conventional finite element approach used here is based on the Galerkin weighted residual method. The equations of motion for each beam are used as the basis of this solution method. Simple harmonic motion is again assumed, and the equations of motion, according to the Euler-Bernoulli beam theory, take the following form:

$$EI_i \frac{\partial^4 \overline{W}_i}{\partial x^4} - EI_i \left(\frac{\lambda_i}{L_i}\right)^4 \overline{W}_i = 0\,, \quad i = 1, \dots 5 \tag{56}$$

where $\overline{W}_i$ is the actual transverse displacement of beam i, and the same non-dimensionalization used in (5) has been applied. An approximate transverse displacement W_i is introduced in place of the actual displacement, such that $W_i \cong \overline{W}_i$. This results in the following residual equation

$$EI_i \frac{\partial^4 W_i}{\partial x^4} - EI_i \left(\frac{\lambda_i}{L_i}\right)^4 W_i = \mathcal{R}\,, \quad i = 1, \dots 5 \tag{57}$$

Then, following the Galerkin method of weighted residuals, this residual is weighted by a virtual displacement, and integrated over the entire domain, the result being set equal to zero, such that:

$$\sum_{i=1}^{5}\left(\int_{0}^{L_i}\left(EI_i\delta W_i W_i'''' - EI_i\left(\frac{\lambda_i}{L_i}\right)^4\delta W_i W_i\right)\mathrm{d}x_i\right) = 0 \tag{58}$$

where $$W_i(x_i) = \langle N_i(x_i)\rangle\{W_n\}$$

The row vector of shape functions, N, depend on the element type being used for analysis and W_n is a column vector of nodal displacements. Integration by parts is then carried out twice, to produce the following:

$$\underbrace{\sum_{i=1}^{5}\left(EI_i[\delta W_i W_i''' - \delta W_i' W_i'']_0^{L_i}\right)}_{*} + \sum_{i=1}^{5}\left(\int_{0}^{L_i}\left(EI_i\delta W_i'' W_i'' - EI_i\left(\frac{\lambda_i}{L_i}\right)^4\delta W_i W_i\right)\mathrm{d}x_i\right) = 0 \tag{59}$$

The term on the left, representing the boundary terms, is also related to the external virtual work $\delta\mathcal{W}_{ext}$, which is imparted to the system by external forces. Since the bending moment is affected by the aforementioned axial force coupling, the boundary term of the above equation can be expressed as For the endpoints of beam sections 1 and 4, the following is true for free vibration:

$$\begin{aligned} EI_1(\delta W_1 W_1''' - \delta W_1' W_1'')|_{x_1=0} &= \delta\mathcal{W}_{ext}|_{x_1=0} \\ EI_5(\delta W_5 W_5''' - \delta W_5' W_5'')|_{x_5=L_5} &= \delta\mathcal{W}_{ext}|_{x_5=L_5} \end{aligned} \tag{60}$$

where $\delta\mathcal{W}_{ext}$ is the external virtual work caused by applied external forces on the system, causing virtual displacements. For the free vibration of this system, the total external work is $\delta\mathcal{W}_{ext} = \delta\mathcal{W}_{ext}|_{x_1=0} + \delta\mathcal{W}_{ext}|_{x_5=L_5} = 0$. The remaining terms in (*) above can be resolved by applying the continuity conditions from (54), with the following as a result:

$$\sum_{i=1}^{5}\left(EI_i[\delta W_i W_i''' - \delta W_i' W_i'']_0^{L_i}\right) = \delta \mathcal{W}_{ext}$$
$$+ \delta W_2(0)\underbrace{\left(EI_1 W_1'''(L_1) - EI_2 W_2'''(0) - EI_3 W_3'''(0) - EI_4 W_4'''(0)\right)}_{**}$$
$$- \delta W_2'(0)\left(EI_1 W_1''(L_1) - EI_2 W_2''(0) - EI_3 W_3''(0) - EI_4 W_4''(0)\right) \quad (61)$$
$$- \delta W_2(L_2)\underbrace{\left(EI_4 W_4'''(0) - EI_2 W_2'''(L_2) - EI_3 W_3'''(L_3) - EI_4 W_4'''(L_4)\right)}_{***}$$
$$+ \delta W_2'(L_2)\left(EI_5 W_5''(0) - EI_2 W_2''(L_2) - EI_3 W_3''(L_3) - EI_4 W_4''(L_4)\right)$$

The terms (**) and (***) in equation (24), as well as the external work term go to zero directly as a result of the shear force continuity conditions. However, the remaining terms do not vanish, since the continuity of bending moments contains an additional implicit bending-axial coupling term, in (53), such that

$$\sum_{i=1}^{5}\left(EI_i[\delta W_i W_i''' - \delta W_i' W_i'']_0^{L_i}\right) = \left(\delta W_2'(L_2) - \delta W_2'(0)\right)\left(\Lambda\left(W_2'(L_2) - \delta W_2'(0)\right)\right) \quad (62)$$

Then, expression (59) becomes:

$$\left[\Lambda\left(\delta W_2'(L_2) - \delta W_2'(0)\right)\left(W_2'(L_2) - W_2'(0)\right)\right]$$
$$+ \sum_{i=1}^{5}\left(\int_0^{L_i}\left(EI_i \delta W_i'' W_i'' - EI_i\left(\frac{\lambda_i}{L_i}\right)^4 \delta W_i W_i\right)\mathrm{d}x_i\right) = 0 \quad (63)$$

Discretizing the domain from into m elements and replacing the displacements above by their equivalent shape function expressions, the following results, which will be the final form of the FEM solution for this formulation:

$$\langle \delta W_n \rangle \Bigg[\left(\{N_2\}'(L_2) - \{N_2\}'(0)\right)\Lambda\left(\langle N_2\rangle'(L_2) - \langle N_2\rangle'(0)\right)$$
$$+ \sum_{\mathrm{i}=1}^{5}\sum_{m=1}^{\#\,elements_i}\left(\int_{x_m}^{x_{m+1}}\left(EI_i\{N_i\}''\langle N_i\rangle'' - EI_i\left(\frac{\lambda_i}{L_i}\right)^4\{N_i\}\langle N_i\rangle\right)\right)\Bigg]\{W_n\} = 0 \quad (64)$$

Thence $$\langle \delta W_n \rangle\left((\mathbf{K} + \mathbf{K_{delam}}) - \omega^2 \mathbf{M}\right)\{W_n\} = \mathbf{0}$$

Appropriate shape functions are then chosen, and substituted into the above to solve for the structural stiffness and mass matrices ($\mathbf{K}$ and $\mathbf{M}$, respectively) and $\mathbf{K_{delam}}$, the delamination stiffness matrix, (*) in equation (64). This yields the same result as the traditional finite element solutions for mass and stiffness ($\mathbf{K} = \int_V [B]^T EI[B]dV$ and $\mathbf{M} = \int_V \{N\}\rho A\langle N\rangle dV$, where $[B]$ is the strain-displacement matrix [33]) with the added stiffness term due to the delamination, and noting that the frequency of excitation squared ω^2 is contained within the non-dimensional frequency term λ^4, which makes this eigenproblem identical to the traditional FEM free vibration problem $[\mathbf{K} - \omega^2\mathbf{M}]\{W_n\} = \mathbf{0}$.

The delamination stiffness can be used in combination with a Boolean term to include or neglect rigid connectors as required without completely redeveloping the system equations. This ability greatly increases the versatility of this method when compared to an analytical solution, or a solution not based on the principle of virtual work.

A further investigation into the effects of higher-order elements was conducted in addition to the refinement of the theory to include multiple delaminations, in order to assess the possible benefits afforded to FEM solutions using higher-order shape functions. The trade-off between increased solution accuracy and solution efficiency was examined in the process.

3.2.1. 2-Node Beam Element

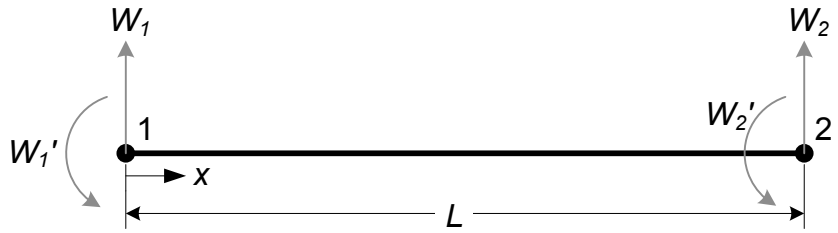

Figure 9 – The 2-node, 4 degree of freedom beam element

The standard Hermite cubic polynomial interpolation functions were chosen to represent a 2-node beam element, with 2 degrees of freedom per node (displacement and slope). The basis functions chosen are linearly independent polynomial bases, up to order 3:

$$W(x) = \langle 1 \quad x \quad x^2 \quad x^3 \rangle \{C\} \tag{65}$$

where {C} is a column vector of unknown constant coefficients. The following represents the vector of nodal displacements used in further FE development:

$$\{W_n\} = \begin{Bmatrix} W_1 \\ W_1' \\ W_2 \\ W_2' \end{Bmatrix} = \begin{bmatrix} 1 & 0 & 0 & 0 \\ 0 & 1 & 0 & 0 \\ 1 & L & L^2 & L^3 \\ 0 & 1 & 2L & 3L^2 \end{bmatrix} \{C\} = [P_n]\{C\} \tag{66}$$

Thus $$W(x) = \langle 1 \quad x \quad x^2 \quad x^3 \rangle [P_n]^{-1} \{W_n\} = \langle \boldsymbol{N} \rangle \{\boldsymbol{W_n}\}$$

These shape functions can then be used in the integral equation provided above to solve for the stiffness and mass matrices. This integration may be carried out symbolically during initial development, or numerically during the solution phase. Due to the relative simplicity of the method, the terms in the stiffness and mass matrix were solved for directly during development. This was true for the second element type, as well.

3.2.2. 3-Node Beam Element

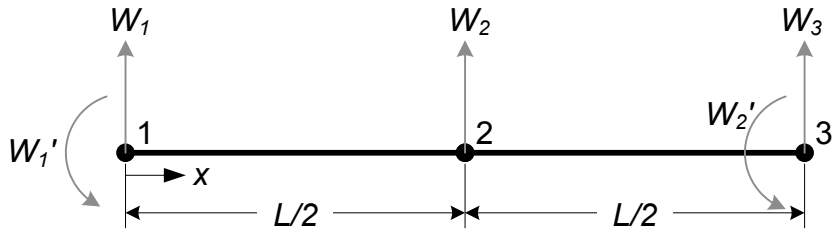

Figure 10 – The 3-node, 5 degree of freedom beam element

Here, the same concept of a polynomial interpolation function is used, as before. However, making use of a higher-order polynomial interpolation functions increases the accuracy of the solution. Whereas for the 2-node beam element a 3rd-order polynomial was required, for a higher-order interpolation of 4th-order one requires the addition of another single degree of freedom to the system. This was accomplished by adding a midpoint node with one degree-of-freedom (lateral displacement) to the beam model used previously. This third node, while increasing the mesh fineness, allows for a greater solution accuracy and possibly

faster convergence, which will be investigated. The 3-node beam element will be developed in the same way as the 2-node beam element, except using the following interpolation function:

$$W(x) = \langle 1 \quad x \quad x^2 \quad x^3 \quad x^4 \rangle \{C\} \tag{67}$$

Consequently, the degrees of freedom for the system will be modified as discussed. The addition of the midpoint node and its associated lateral degree of freedom are compensated for by using the following degrees of freedom:

$$\{W_n\} = \begin{Bmatrix} W_1 \\ W_1' \\ W_2 \\ W_3 \\ W_3' \end{Bmatrix} = \begin{bmatrix} 1 & 0 & 0 & 0 & 0 \\ 0 & 1 & 0 & 0 & 0 \\ 1 & L/2 & L^2/4 & L^3/8 & L^4/16 \\ 1 & L & L^2 & L^3 & L^4 \\ 0 & 1 & 2L & 3L^2 & 4L^3 \end{bmatrix} \{C\} = [P_n]\{C\} \tag{68}$$

Thus $$W(x) = \langle 1 \quad x \quad x^2 \quad x^3 \quad x^4 \rangle [P_n]^{-1} \{W_n\} = \langle \boldsymbol{N} \rangle \{\boldsymbol{v_n}\}$$

3.3. Dynamic Stiffness Matrix (DSM) Formulation

Although the analytical solution presented above fulfils the initial requirements of this project, some transformations can still be made to make the solution process more intuitive and extensible. To this end, the concept of a Dynamic Stiffness Matrix (DSM) will be utilized. Whereas the analytical solution is self-contained and relies on the solution of a coefficient matrix, the DSM approach results in a more useful, force-displacement relationship. This can then be used for the same purpose as the initial approach – solving a free vibration problem at the delamination level – or the problem can be extended, using other dynamic finite elements. This allows for a greater breadth of analysis, since the delamination configuration is not limited to simple intact-delaminated-intact beam segments.

Using the requirement for a force-displacement relationship with the already established general solution, we can use the standard, beam theory descriptions of internally developed bending moment and shear stress as:

$$M_i = EI_i \frac{d^2 W_i(x_i)}{dx_i^2}$$
$$S_i = EI_i \frac{d^3 W_i(x_i)}{dx_i^3} \tag{69}$$

Then, the following can be substituted into the above, noting again the general solution to the differential equations of motion:

$$\begin{aligned}
W_i(x_i) &= \left[\cos\left(\lambda_i \frac{x_i}{L_i}\right) \quad \sin\left(\lambda_i \frac{x_i}{L_i}\right) \quad \cosh\left(\lambda_i \frac{x_i}{L_i}\right) \quad \sinh\left(\lambda_i \frac{x_i}{L_i}\right)\right]\{C_i\} \\
\frac{\mathrm{d}W_i(x_i)}{\mathrm{d}x} &= \frac{1}{L_i}\left[-\sin\left(\lambda_i \frac{x_i}{L_i}\right) \quad \cos\left(\lambda_i \frac{x_i}{L_i}\right) \quad \sinh\left(\lambda_i \frac{x_i}{L_i}\right) \quad \cosh\left(\lambda_i \frac{x_i}{L_i}\right)\right]\{C_i\} \\
\frac{\mathrm{d}^2 W_i(x)}{\mathrm{d}{x_i}^2} &= \left(\frac{1}{L_i}\right)^2 \left[-\cos\left(\lambda_i \frac{x_i}{L_i}\right) \quad -\sin\left(\lambda_i \frac{x_i}{L_i}\right) \quad \cosh\left(\lambda_i \frac{x_i}{L_i}\right) \quad \sinh\left(\lambda_i \frac{x_i}{L_i}\right)\right]\{C_i\} \\
\frac{\mathrm{d}^3 W_i(x)}{\mathrm{d}{x_i}^3} &= \left(\frac{1}{L_i}\right)^3 \left[\sin\left(\lambda_i \frac{x_i}{L_i}\right) \quad -\cos\left(\lambda_i \frac{x_i}{L_i}\right) \quad \sinh\left(\lambda_i \frac{x_i}{L_i}\right) \quad \cosh\left(\lambda_i \frac{x_i}{L_i}\right)\right]\{C_i\}
\end{aligned} \tag{70}$$

where $\{C_i\}$ is a column vector of constant coefficients. Since the delamination tips will be the boundaries of the domain of interest, the bending moment definition is modified from that provided by beam theory to account for the bending-axial coupling described previously. The proper definitions for bending moment and shear force at the delamination tips then become:

$$\begin{aligned}
M_1 &= EI_2 W_2'' + EI_3 W_3'' + EI_4 W_4'' + \Lambda\left(W_1'(x_1 = L_1) - W_5'(x_5 = 0)\right) \\
S_1 &= EI_2 W_2''' + EI_3 W_3''' + EI_4 W_4'''
\end{aligned} \tag{71}$$

where $(\cdot)'$ represents the differentiation with respect to the beam longitudinal axis, *x*. Similar relationships can be derived for the second endpoint, using the previously identified relationships. Creating a column vector of nodal forces, we have the following:

$$\begin{Bmatrix} S_1 \\ M_1 \\ S_2 \\ M_2 \end{Bmatrix} = \mathbf{F} = \boldsymbol{A_2}\{C_2\} + \boldsymbol{A_3}\{C_3\} + \boldsymbol{A_4}\{C_4\} \tag{72}$$

where $\boldsymbol{A_2}$, $\boldsymbol{A_3}$ and $\boldsymbol{A_4}$ contain the frequency dependent coefficients of the unknown constants for beams 2, 3, and 4, respectively. Then, assuming some relationship can be found that relates

the unknown constants of beams 3 and 4 to those of 2 (which will be described later) by $\{C_3\} = \boldsymbol{B_{32}}\{C_2\}$, $\{C_4\} = \boldsymbol{B_{42}}\{C_2\}$, then:

$$\mathbf{F} = (\boldsymbol{A_2} + \boldsymbol{A_3}\boldsymbol{B_{32}} + \boldsymbol{A_4}\boldsymbol{B_{42}})\{C_2\} \tag{73}$$

Since this development makes use of nodal displacements, nodes 1 and 2 are defined at the left and right endpoints, respectively, of the delaminated beam model, then the following is also true:

$$W_2(x_2 = 0) = W_3(x_3 = 0) = W_4(x_4 = 0) = [1 \quad 0 \quad 1 \quad 0]\{C_{2,3,4}\}$$

Similar continuity conditions for *W'₁*, *W₂*, and *W'₂* exist at each delamination tip. This gives the following relationship between nodal displacements and constant coefficients (using the coefficients for beam 2 as a reference):

$$\begin{Bmatrix} W_1 \\ W_1' \\ W_2 \\ W_2' \end{Bmatrix} = \begin{bmatrix} 1 & 0 & 1 & 0 \\ 0 & 1 & 0 & 1 \\ C_{\lambda_2} & S_{\lambda_2} & Ch_{\lambda_2} & Sh_{\lambda_2} \\ -\frac{\lambda_2}{L_2}S_{\lambda_2} & \frac{\lambda_2}{L_2}C_{\lambda_2} & \frac{\lambda_2}{L_2}Sh_{\lambda_2} & \frac{\lambda_2}{L_2}Ch_{\lambda_2} \end{bmatrix}\{C_2\} \tag{74}$$

$$\mathbf{u} = \boldsymbol{D_2}\{C_2\}$$

where $C_{\lambda_2} = \cos(\lambda_2)$, $S_{\lambda_2} = \sin(\lambda_2)$, $Ch_{\lambda_2} = \cosh(\lambda_2)$, $Sh_{\lambda_2} = \sinh(\lambda_2)$. Combining this with the force relationship, from equation (73), the following can be shown:

$$\begin{gathered} \mathbf{F} = (\boldsymbol{A_2} + \boldsymbol{A_3}\boldsymbol{B_{32}} + \boldsymbol{A_4}\boldsymbol{B_{42}})\boldsymbol{D_2^{-1}}\mathbf{u} \\ \mathbf{F} = \mathbf{K}\mathbf{u} \end{gathered} \tag{75}$$

where $\mathbf{K}$ is the system stiffness matrix, whose elements are all dynamic in nature, functions of frequency. This system equation is in the proper form for use with other elements, as was intended from the start. Free vibration occurs when the determinant of this stiffness matrix vanishes.

As previously described, the form of the system stiffness matrix is dependent on the existence of some coupling relationship between the unknown constants for beams 3 and 4 with respect to those for beam 2. Using the concept of nodal displacements described above, the following is true for each beam, with the vector **u** being identical in each case, since the transverse displacement and slope are continuous across the endpoints at which $\mathbf{u}|_{\text{element n}}$ is defined:

$$\mathbf{u}|_{\text{element 2}} = \boldsymbol{D_2}\{C_2\}\,, \qquad \mathbf{u}|_{\text{element 3}} = \boldsymbol{D_3}\{C_3\}\,, \qquad \mathbf{u}|_{\text{element 4}} = \boldsymbol{D_4}\{C_4\} \tag{76}$$

where u_i represent the column vector of nodal displacements for beam i, D_i is the matrix of coefficients for beam i, and $\{C_i\}$ represents the unknown constants for beam i. At the delamination tips, in order to ensure inter-element continuity of displacements and their first derivatives (C^1 continuity), the displacements and their first derivatives are equal for each delaminated beam. Since these displacements and slopes also represent the nodal displacements and slopes W_i, it can be shown that:

$$\begin{aligned} \mathbf{u}|_{\text{element 2}} = \mathbf{u}|_{\text{element 3}}\,, &\qquad \mathbf{u}|_{\text{element 2}} = \mathbf{u}|_{\text{element 4}} \\ \boldsymbol{D_2}\{C_2\} = \boldsymbol{D_3}\{C_3\}\,, &\qquad \boldsymbol{D_2}\{C_2\} = \boldsymbol{D_4}\{C_4\} \\ \{C_3\} = \boldsymbol{D_3^{-1}D_2}\{C_2\}\,, &\qquad \{C_3\} = \boldsymbol{D_3^{-1}D_2}\{C_2\} \end{aligned} \tag{77}$$

Thus $$\boldsymbol{B_{32}} = \boldsymbol{D_3^{-1}D_2}\,, \qquad \boldsymbol{B_{42}} = \boldsymbol{D_4^{-1}D_2}$$

which satisfies the initial requirement that the $\boldsymbol{B_{ij}}$ matrices exist, and also gives the explicit form of these coupling matrices. All terms within the stiffness matrix have now been identified, and the free vibration modes of the system can be solved using this newly developed $\mathbf{K}$, together with root solving algorithms, to satisfy the free vibration condition that $\mathbf{Ku} = \mathbf{0}$, if and only if $\det(\mathbf{K}) = 0$.

3.4. Dynamic Finite Element (DFE) Formulation

Due to the accuracy of the 2-node DFE beam element observed (see Contributions 1-6 in Section 6, and the results discussed in the next Section) in the single delamination formulation, it was not necessary to develop a 3-node DFE element in the double-delamination case. The formulation presented here will be for a 2-node, 2 degree-of-freedom per node beam element (4-DOF), with the same coordinate system and definitions presented in Figure 9. The weak form of the weighted residual formulation from the FEM development (expression (63)), is

$$\begin{aligned}&\left[\Lambda\left(\delta W_2'(L_2)-\delta W_2'(0)\right)\left(W_2'(L_2)-W_2'(0)\right)\right]\\&\quad+\sum_{i=1}^{5}\left(\int_0^{L_i}\left(EI_i\delta W_i''W_i''-EI_i\left(\frac{\lambda_i}{L_i}\right)^4\delta W_iW_i\right)\mathrm{d}x_i\right)=0\end{aligned}\tag{78}$$

The domain is then discretized over a number of elements ($\#\ elements_i$), and another set of integrations by parts is performed. The result of this is the following, where the order of differentiation of the displacement W_i and the virtual displacement, δW_i, have been reversed from the original weighted residual formulation:

$$\begin{aligned}&\Lambda\left(\delta W_2'(L_2)-\delta W_2'(0)\right)\left(W_2'(L_2)-\delta W_2'(0)\right)\\&\quad+\sum_{i=1}^{5}\sum_{m=1}^{\#\ elements_i}\left(EI_i[\delta W_i''W_i'-\delta W_i'''W_i]_{x_m}^{x_{m+1}}\right.\\&\quad\left.+\int_{x_m}^{x_{m+1}}\left(\underbrace{EI_i\delta W_i''''W_i-EI_i\left(\frac{\lambda_i}{L_i}\right)^4\delta W_iW_i}_{*}\right)dx\right)=0\end{aligned}\tag{79}$$

For the DFE formulation, the interpolation functions are chosen such that the expression (*) above goes to zero with the approximation implemented. Thus, the general solution to (*) was chosen to be the basis functions from which shape functions would be derived, much in the same way as the single delamination DFE was implemented. Since beam sections 1-5 would be independent within their own unique sub-domains, each could be meshed using elements with different shape functions, with no effect on the finite element assembly, so long as the

delamination stiffness implementation – (*) in the expression above – is implemented properly. For an uncoupled Euler-Bernoulli beam, the interpolation functions take the following form

$$W_i(\xi_i) = \left\langle \cos(\alpha_i\xi_i) \quad \frac{\sin(\alpha_i\xi_i)}{\alpha_i} \quad \frac{\cosh(\alpha_i\xi_i) - \cos(\alpha_i\xi_i)}{{\alpha_i}^2} \quad \frac{\sinh(\alpha_i\xi_i) - \sin(\alpha_i\xi_i)}{{\alpha_i}^3} \right\rangle \{C_i\} \\ = \langle \boldsymbol{P_i} \rangle \{\boldsymbol{C_i}\} \tag{80}$$

where $\{C_i\}$ is a column vector of constant coefficients, ξ_i is the non-dimensional axial coordinate, x_i/L_i , and α_i is a constant coefficient, equal to

$$\alpha_i = \frac{\omega^2 \rho_i A_i}{EI_i} \tag{81}$$

In much the same way as the interpolation functions were found for the single delamination formulation, the form that was adopted is a linear combination of the linearly independent interpolation functions introduced in (4), such that they collapse to the Hermite cubic interpolation functions as the frequency of excitation approaches zero. The shape functions were found using the following:

$$\{W_n\} = \begin{Bmatrix} W_i(\xi_i = 0) \\ W_i'(\xi_i = 0) \\ W_i(\xi_i = 1) \\ W_i'(\xi_i = 1) \end{Bmatrix} = \begin{bmatrix} 1 & 0 & 0 & 0 \\ 0 & 1 & 0 & 0 \\ \cos(\alpha_i) & \frac{\sin(\alpha_i)}{\alpha_i} & \frac{\cosh(\alpha_i) - \cos(\alpha_i)}{{\alpha_i}^2} & \frac{\sinh(\alpha_i) - \sin(\alpha_i)}{{\alpha_i}^3} \\ -\alpha sin(\alpha_i) & \cos(\alpha_i) & \frac{\alpha\sinh(\alpha_i) + \alpha\sin(\alpha_i)}{{\alpha_i}^2} & \frac{\alpha\sinh(\alpha_i) - \alpha\cos(\alpha_i)}{{\alpha_i}^3} \end{bmatrix} \\ = [\boldsymbol{P_n}]_i \{\boldsymbol{C_i}\} \tag{82}$$

thus

$$W_i(\xi_i) = \langle P \rangle [P_n]_i^{-1} \{W_n\} = \langle \boldsymbol{N_i} \rangle \{\boldsymbol{W_n}\}, \tag{83}$$

where $\{(\cdot)_n\}$ represents the nodal values at the endpoints of the beam element. It should be noted also that, while the coordinate non-dimensionalization to ξ_i was made, the differentiation is still with respect to x_i , and this should be respected in the formulation. Introducing the shape functions back into the discretized equation, the following results:

$$\langle \delta W_n \rangle \Bigg(\big(\{N_2\}'(L_2) - \{N_2\}'(0)\big)\Lambda\big(\langle N_2\rangle'(L_2) - \langle N_2\rangle'(0)\big) + \sum_{i=1}^{5} \sum_{m=1}^{\#\, elements_i} \big(EI_i[\{N_i\}''\langle N_i\rangle' - \{N_i\}'''\langle N_i\rangle]_{x_m}^{x_{m+1}}\big) \Bigg) \{W_n\} = 0, \tag{84}$$

or $$\langle \delta W_n \rangle (\mathbf{K_{DFE}} + \mathbf{K_{delam}}) \{W_n\} = 0$$

where $\mathbf{K_{DFE}}$ is the frequency-dependent structural stiffness matrix, and $\mathbf{K_{delam}}$ is the delamination stiffness matrix, from the conditions imposed at the delamination tips. The above statement is true if and only if

$$\det(\mathbf{K_{DFE}} + \mathbf{K_{delam}}) = 0$$

This process gives a platform from which solutions may be obtained. Either traditional eigensolvers, coupled with frequency-sweeping, or more advanced root finding algorithms [53]. This gives the DFE formulation more flexibility over a traditional FEM-based solution alone, in that more solver types are available, depending on the form of the problem at hand.

The similarities between this formulation and the previous, single delamination formulation should be apparent, and this is an important note. The analytical formulation had to expand to include additional conditions and equations in this formulation, but the fundamental application of the DFE theory remained the same across applications. This is more evidence of the utility of the DFE formulation; different scenarios, which might require a large-scale expansion of the solution algorithm (for example, by introducing extra delamination conditions in an analytical formulation), may be handled relatively easily using a DFE approach. This ease of transitioning between test cases is one of the prime motivators for FEM-based techniques, and DFE combines this advantage with the frequency-based approach that DSM and analytical techniques use for increased solution accuracy with fewer (in the case of DSM) elements.

3.5. Numerical Tests

In order to assess the accuracy of the proposed solution method, a series of different delamination configurations will be analyzed using the methods outlined above. Results obtained from an analytical solution and those gathered from the literature will be presented and compared to this method to achieve such assessment. Note that the boundary conditions are clamped-clamped.

Since the models presented in this section are relatively simple and computation time is not relevant to the analysis, the following discretization – which may not be optimized for fast solution speeds – was used to mesh the domains presented below (see Appendix C a discussion on the numerical sensitivity of this mesh):

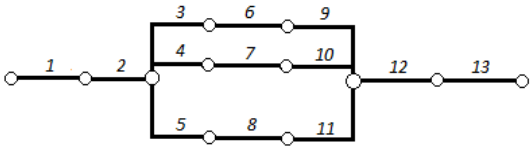

Figure 11 – Mesh discretization for double-delaminated configurations

3.5.1. Model 1 Frequency Results

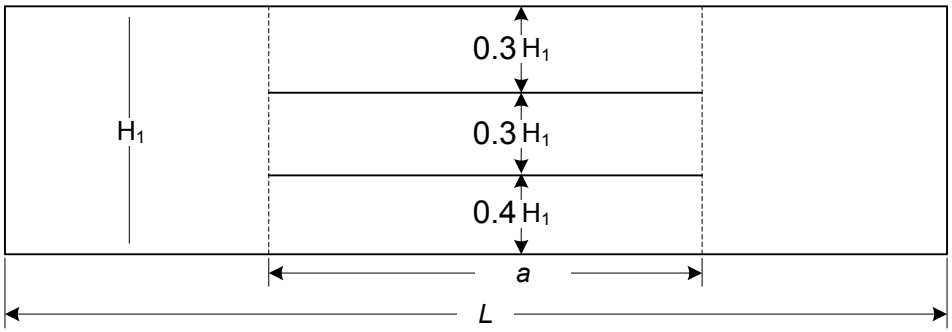

Figure 12 - The first double-delamination model

The first delamination model tested is illustrated in the figure above. The top and centre delaminated beams each have a height of 30% the intact beam height. In addition, the delamination length, a, was varied as a percentage of the total beam length from 20% to 50%. The delamination is central, meaning that the left and right intact segments have equal lengths.

The frequency results for these delaminated clamped-clamped beam configurations are presented in Table 5. The results include those from the literature [17], which have been interpolated from a graph.

Table 5 – The first and second nondimensional frequency parameter λ^2 for model 1

a/L	Ref [17]	2-Node FEM	3-Node FEM	Exact/ Analytical	DSM	DFE	
0.2	4.7	4.725	4.725	4.725	4.725	4.725	
0.3	4.7	4.691	4.695	4.695	4.695	4.695	Mode
0.4	4.6	4.574	4.572	4.575	4.575	4.575	1
0.5	4.3	4.318	4.315	4.315	4.315	4.315	
0.2	7.1	7.054	7.046	7.045	7.045	7.045	
0.3	6.3	6.337	6.334	6.335	6.335	6.335	Mode
0.4	6.0	5.965	5.960	5.965	5.965	5.965	2
0.5	5.9	5.860	5.846	5.845	5.845	5.845	

When it comes to conventional FEM frequency results, it can be observed from Table 5 that both 2- and 3-node beam elements perform well with respect to both the analytical solution, as well as those taken from the literature. Slight deviations (0.26% for 2-node mode 2, with respect to the exact/analytical solution) are present for larger delamination sizes and for higher modes of vibration, as it was expected from the start of FEM development.

Similarly, the same trend can be observed here as was present during the sensitivity analysis. For higher modes, the 3-node beam tended to perform better than the 2-node beam (albeit only slightly). This difference is expected to increase with an increase in mode number. However, for the first mode and for small delamination sizes, the 2- and 3-node beam elements perform similarly and differences between the results for each element were negligible. This could be used to justify the use of a 2-node beam element in such situations to save on processor requirements and solution times.

Excellent agreement can be seen between the dynamic element-based solution methods (DSM and DFE) and the exact (analytical) solution method (Table 5). This was again expected, since the element-based solution was built upon the same general solution to the differential equation of motion from which the analytical solution was derived. This would

change if more complexities were added to the system, including coupled displacements or non-constant material or geometric properties. In these cases, analytical solutions would be cumbersome (if not impossible) to find, but it would be expected that DFE and DSM results would diverge from each other for low element counts, as DSM takes advantage of certain simplifying assumptions (see [2-9] for more detail) to allow the coupled equations to be expressed in a very particular form, while a DFE formulation would treat coupled and uncoupled parts of the set of equations separately, like FEM-based techniques. Even for these cases, for a finer DFE mesh, it has been shown that DSM and DFE do correlate well (for example, [22]), lending further confidence to the use of these techniques.

3.5.2. Model 1 Mode Shapes

The vibration mode shapes are also an important consideration in free vibration modeling. Identifying nonphysical or physically inadmissible behaviour can be essential in improving a given model. To that end, the mode shapes for the first two modes above were compiled. These were generated from the eigenvector result corresponding to the eigenvalue, which represented a particular fundamental frequency. This mode shape was used to determine the lateral displacement, $w(x)$, as a function of the axial coordinate, x, from the shape functions derived earlier.

Since the variance between mode shapes for the 2- and 3-node beam elements was minimal, only the mode shape for the 3-node beam will be plotted. Additionally, using the exact solution presented in the preceding sections, the exact mode shapes were determined and plotted as another point of comparison to verify the utility of the present method.

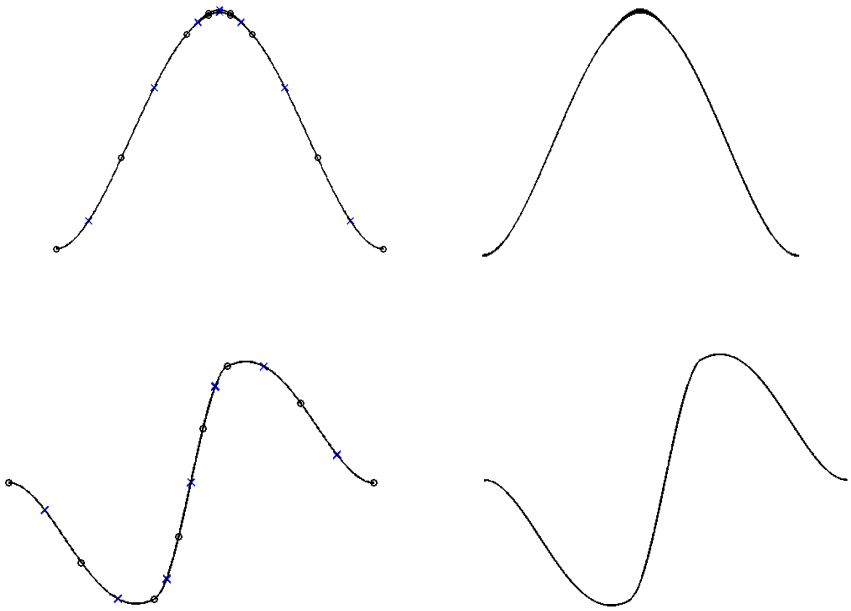

Figure 13 - Model 1 mode shapes for a/L = 0.2.

Top: mode 1; Bottom: mode 2; Left: FEM; Right: Exact

Note that in the figure above, the element end nodes are represented by circular markers, and the midpoint nodes are represented by X markers. The mode shapes generated using the present method are quite close in shape to those generated from the exact solution. Some loss in fidelity of the FEM beam shapes can be attributed to the quartic (or cubic, for 2-node beam elements) shape functions, approximating the trigonometric and hyperbolic functions representing the exact solution. The DFE mode shapes, not shown here for brevity, were found to be almost identical (within a few pixels) to the FEM ones. See Appendix B for additional FEM and analytical double-delamination mode shapes for different delamination lengths.

3.5.3. Model 2 Frequency Results

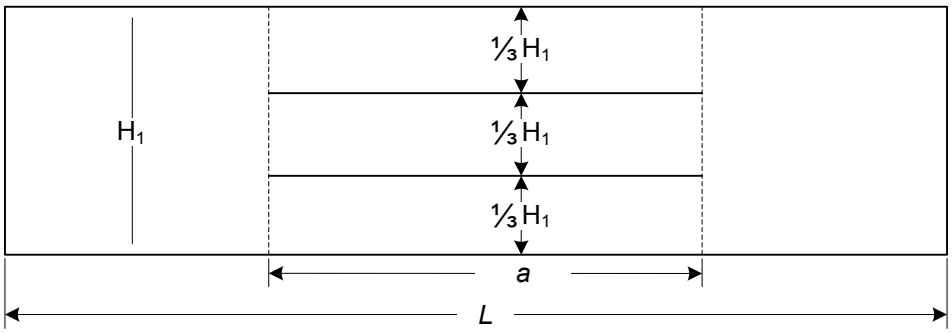

Figure 14 - The second double-delamination model

Another delamination model used for verification from [5] is illustrated above. The delaminated beams have the same height, equal to one third of the intact beam height. As before, the results reported from [17] were converted from chart to numerical form. The final results of this second analysis are detailed below (Table 6).

Table 6 – The first and second nondimensional frequency parameter λ^2 for model 2

a/L	Ref [17]	FEM 2-Node	FEM 3-Node	Exact	DSM	DFE	
0.2	4.7	4.726	4.725	4.725	4.725	4.725	
0.3	4.7	4.692	4.695	4.695	4.695	4.695	Mode
0.4	4.6	4.580	4.578	4.575	4.575	4.575	1
0.5	4.3	4.342	4.338	4.335	4.335	4.335	
0.2	7.0	7.010	7.002	7.005	7.005	7.005	
0.3	6.3	6.284	6.281	6.285	6.285	6.285	Mode
0.4	5.9	5.922	5.917	5.915	5.915	5.915	2
0.5	5.8	5.833	5.820	5.815	5.815	5.815	

It can be observed that for smaller delamination sizes, the 2-node and 3-node beam elements performed with similar accuracy, and both converged to a reasonable accuracy (largest deviation approximately 0.16% from the exact solution). However, for higher modes and larger delamination sizes, the 3-node beam exhibits higher accuracy and better convergence characteristics, as detailed in the sensitivity analysis contained in Appendix C.

Once again, excellent agreement was observed between the frequency-based element solutions (DSM and DFE) and the exact (analytical) solutions. Furthermore, these results were

obtained with only slight modifications to the single delamination technique presented earlier. While the analytical solution had to be completely modified, DSM and DFE development very closely followed the same process as outlined before. This lends further credence to the advantages of these formulations, since good correlation with analytical results can be achieved with less development overhead. The usage of DFE or DSM to compute results for more complex cases might achieve similar accuracy, where analytical solutions might be significantly more difficult to obtain, if not impossible to obtain without approximation.

3.5.4. Model 2 Mode Shapes

The same principle was used to find the mode shapes for model 2, as well. The first mode shapes are presented here and, for brevity, additional FEM and analytical double-delamination mode shapes are contained in Appendix A for different delamination lengths.

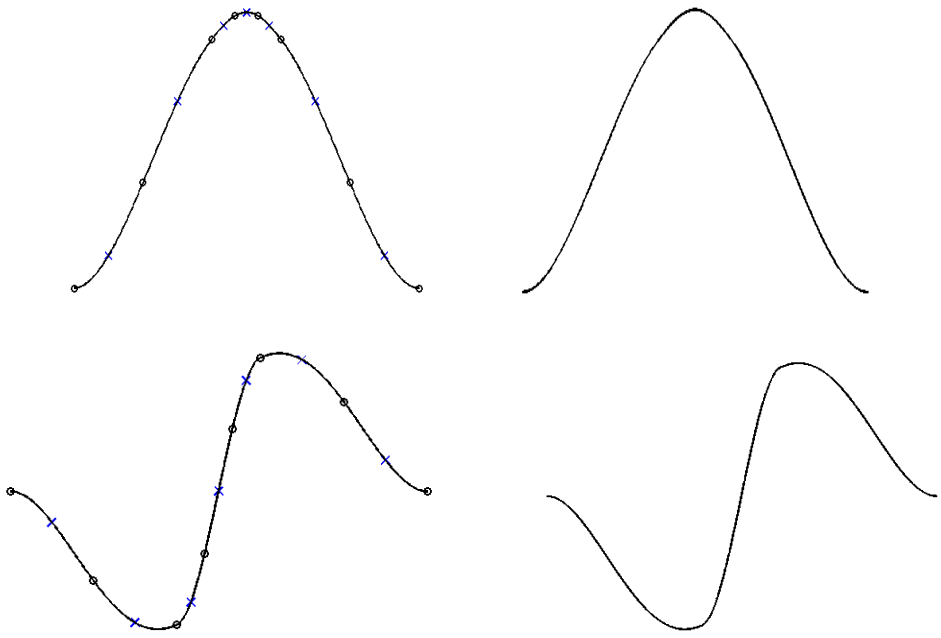

Figure 15 – Model 2 mode shapes for a/L = 0.2.

Top: mode 1; Bottom: mode 2; Left: FEM; Right: Exact

Similarly, the mode shapes for model 2 are similar when comparing the FEM model with the exact model. Discrepancies again can be mainly attributed to the use of polynomials to interpolate for trigonometric and hyperbolic functions, but the differences are slight and almost

indistinguishable when examining the mode shapes by eye. Again, the FEM model highlights beam end nodes with circular markers and midpoint nodes with **X** markers. The DFE mode shapes, not shown here for brevity, were found to be almost identical to the FEM ones. See Appendix A for the additional double-delamination mode shapes for different delamination lengths.

3.5.5. Physically Inadmissible Modes

Some mode shapes emerged from the analysis, which involved physically inadmissible mode shapes. In this case, the inadmissibility came from the interpenetration of different beam layers with each other (see Figure 9). That is, one beam segment would vibrate laterally in one direction and another beam segment, occupying the same axial domain, would vibrate laterally in the opposite direction. The physically inadmissible mode shapes found for normal vibration occur when the difference in flexural stiffness of the beams is nonzero, and worsens with increasing difference. Since this is purely a physical phenomenon, it can be seen for all exact, DSM, DFE and FEM solutions. It was observed that if the difference in beam stiffness between the three delaminated beams were sufficiently large, these modes would appear to be slight interpenetrations.

Also, some mode shapes, corresponding to system global poles, or partial (off-delamination) poles, emerged from the DFE modeling presented here. The poles are a result of the denominator of the stiffness matrix (and shape functions) vanishing. Since the interpolation are known, an expression for the frequencies corresponding to the system poles, and therefore the number of such frequencies laying below any frequency value, can be found. This can then be used in more advanced root solving techniques, such as Wittrick-Williams [53], to increase solution speeds.

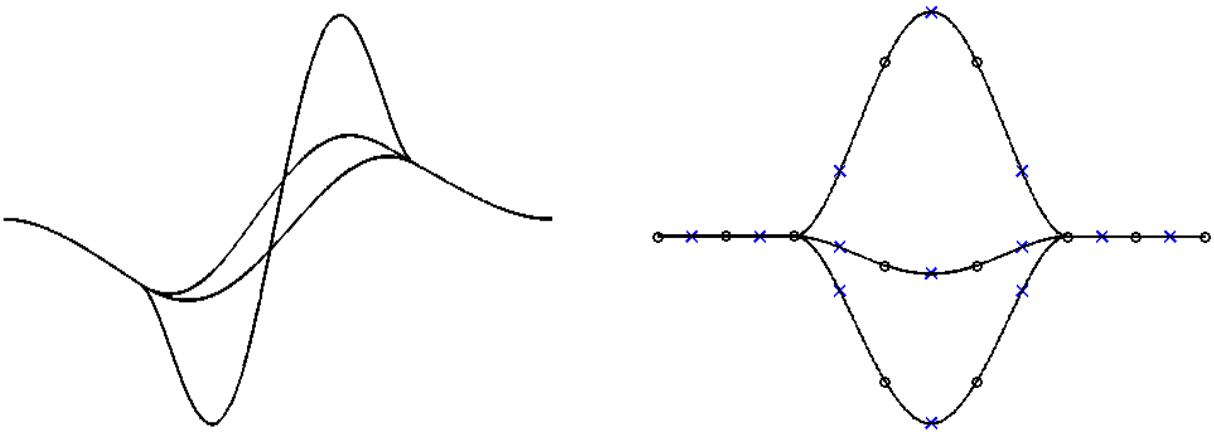

Figure 16 - Examples of physically inadmissible mode shapes. $H_2 = 0.3H_1$, $H_3 = 0.5H_1$, a/L = 0.5

Left: interpenetration due to natural vibration. 4th mode, $\lambda^2 = 5.96$

Right: off-delamination level partial pole 2nd mode, $\lambda^2 = 4.67$

4. Verification Using Commercial FEM Software

The theoretical development of a model for predicting the vibration behaviour of delaminated beams has been presented, and validated according to results obtained by other researchers and those in the literature. However, in order to further validate the theoretical approach, it was necessary to use contemporary engineering tools to model the system and estimate the resulting behaviour. To this end, the frequency results reported by J. Bellcave [11], obtained using a commercial FEM software package, ANSYS® 10 and its built-in element library, was utilized as a basis for comparison. Two different approaches were used to predict vibration behaviour within the commercial FEM environment – a beam element-based model, and a 2D planar element-based model. The accuracy of the presented theory with respect to each model will be presented below.

4.1. Beam Model

The first approach used beam elements to model the system, which was natural since the analytical, DSM, DFE, and FEM solutions all utilized Euler-Bernoulli beams in their fundamental assumptions. Using the ANSYS® element library, the BEAM3 element (2-node, 3 degree-of-freedom per node, linear, elastic beam) was used to mesh the intact and delaminated sections. The beam elements' locations were generated according to where the neutral axis locations of the respective beam sections. In order to enforce the kinematic delamination conditions across the delamination tips, built-in ANSYS® MPC184 elements (multipoint constraint elements) were used, which enforced the continuity requirements at those points. The system, as represented in the FEM software, is shown below.

Figure 17 – Beam ANSYS© model of a delaminated beam [11]

Visible at the endpoints of the model in Figure 17 are the clamped-clamped constraints found in the literature, which were used here for an accurate assessment of the performance of the FEM model created using commercial software.

Convergence was determined by using different element sizing to generate the above mesh. A convergence to less than 0.5% error was satisfied using element lengths equal to 1% the total system length. It is important to note that using the BEAM3 element, axial effects are included, whereas these are estimated [35] in the presented theory. Thus, any axial-bending coupling effects from the inclusion of an axial degree of freedom not accurately captured by the estimate used by Mujumdar [35] would cause a discrepancy in the modal solution. The standard ANSYS® Block-Lanczos solver (without any pre-stressing or added mass) was used to solve for the natural frequencies and mode shapes of the system.

4.2. 2D Model

Another approach exploited to model the delaminated system in ANSYS® was using 2-dimensional elements. This would provide a closer approximation to reality, while still having basis assumptions and constraint types which were consistent enough with beam theory to be used for comparison. It was noted that the differences between the two theories would result in some solution discrepancies.

2-dimensional element PLANE182 (4-node, 2 degree-of-freedom per node, linear, elastic quadrilateral) was used to model the system. The system was modeled as two fully delaminated beams, which were then constrained at their interface to have equal displacements where the intact sections were found. The same MPC184 (multipoint constraint) elements were used for this purpose as were used previously to constrain the delamination tips. This effectively reproduced the intact sections with no loss in system fidelity. The system, as represented in the FEM software [11], is shown below.

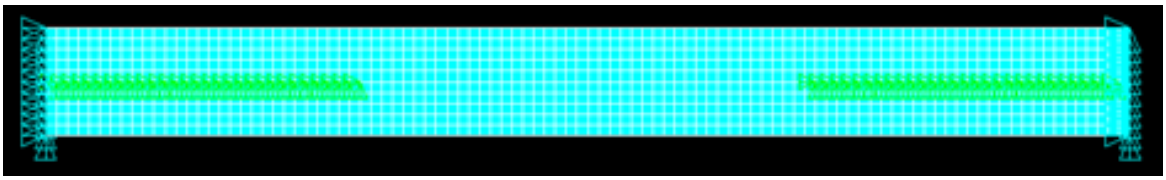

Figure 18 – 2D ANSYS® model of a delaminated beam [11]

The same clamped-clamped constraints used previously are visible in Figure 18, where each node along the tip to be constrained has the constraint applied. Also visible are the

multipoint constraints along the delamination interfaces of those sections, which were made to behave as intact beam sections.

For convergence analysis of the 2D elements, the same approach was used as was used for beam element sizing [11]. Element sizes were set to be square (or as close to an aspect ratio of 1.0 as possible, taking into account the beam height may not be an integer multiple of the length fraction used to size the beam elements), with edge lengths set equal to some fraction of the system length. An element edge length equal to 0.1% of the intact system length yielded convergence to less than 0.3% error. This convergence did not represent solution accuracy, however, as this will be discussed further below. As with the beam model, the standard ANSYS® Block-Lanczos solver (without any pre-stressing or added mass) was used to solve for the natural frequencies and mode shapes of the system.

Solution accuracy is expected to be affected by a number of factors. First, and most importantly, Bellcave did not respect the required minimum length-to-height ratio (L/H>10) to satisfy the Euler-Bernoulli beam assumption; the L/H>10 condition must be satisfied for all the beam segments within the delaminated model. In addition, the 2D modeled system does not explicitly utilize rigid delamination faces. The originally planar faces normal to the beam neutral axes at the delamination tips are assumed to remain planar and normal to the neutral axes (from the Euler-Bernoulli assumptions) after deformation. Instead, the delamination faces are 'soft', and can deform as necessary to minimize the potential energy of the deformed system. The lack of a rigid connector could also reduce the stiffness of the system when compared to the beam theory models. Thus, a reduction in the natural frequencies found here is expected.

4.3. ANSYS® Results

Both the beam and 2D models were used to find the first two natural frequencies and mode shapes of the system, in order to compare to those results found in the literature [17] for equivalent delaminated beam systems. The results for each model will be presented separately, including convergence information. In each case, to better compare with the literature, the normalized natural frequency λ^2 was used, where

$$\lambda^2 = \frac{\omega^2 \rho_0 A_0}{EI_0} L_0^4$$

where ρ_0, A_0, EI_0, and L_0 are the linear mass density (mass per unit length), cross-sectional area normal to the undeformed neutral axis, bending stiffness, and length of the equivalent intact system, respectively and ω is the frequency of excitation.

4.3.1. Beam Model

The variation in natural frequency with delamination length is shown below. The delamination length a was normalized with respect to the equivalent intact beam length L_0.

Table 7 – The variation in natural frequency for a beam element model, fom [11]

	First Mode					Second Mode				
$\frac{a}{L_0}$	Elem size 1%L	Elem size 0.1%L	Della & Shu [17]	Wang, et al. [49]	DSM/ DFE	Elem size 1%L	Elem size 0.1%L	Della & Shu [17]	Wang, et al. [49]	DSM/ DFE
0.1	22.25	22.25	22.37	22.37	22.37	59.74	59.74	60.76	60.76	60.80
0.2	22.24	22.24	22.36	22.35	22.36	55.29	55.29	55.97	55.97	55.99
0.3	22.12	22.12	22.24	22.23	22.24	48.48	48.48	49.00	49.00	49.00
0.4	21.72	21.729	21.83	21.83	21.83	43.31	43.31	43.87	43.87	43.89
0.5	20.80	20.80	20.89	20.88	20.89	40.80	40.80	41.45	41.45	41.52
0.6	19.22	19.22	19.30	19.29	19.30	40.21	40.21	40.93	40.93	41.03

Very good agreement can be seen between the beam-based finite element models generated using commercial FEM software and the beam-based analytical solutions from the literature. This was to be expected and, in fact, the FEM formulation performed in Section 2 provided evidence of this, even if it was not a traditional FEM formulation, as ANSYS® provided. Slight discrepancies can be noted, and are likely due to the application of delamination conditions. In the formulation presented in the literature, axial displacements are accounted for implicitly through approximate techniques [35]. The imposition of axial displacements added additional constraints to the system, tending to increase the system stiffness, and hence increase the natural frequencies seen in the literature. Still, these discrepancies were small (less than 2%), and the results verified the theory presented using industry-standard definitions and implementations of FEM.

4.3.2. 2D Model

The same delamination length normalization was used here, where the delamination length a was normalized with respect to the equivalent intact beam length L_0.

Table 8 – The variation in natural frequency for a 2D element model, fom [11]

	First Mode					Second Mode				
$\frac{a}{L_0}$	Elem size 1%L	Elem size 0.1%L	Della & Shu [17]	Wang, et al. [49]	DSM/ DFE	Elem size 1%L	Elem size 0.1%L	Della & Shu [17]	Wang, et al. [49]	DSM/ DFE
0.1	21.31	21.25	22.37	22.37	22.37	54.01	54.11	60.76	60.76	60.80
0.2	21.28	21.23	22.36	22.35	22.36	49.59	49.98	55.97	55.97	55.99
0.3	21.13	21.09	22.24	22.23	22.24	44.16	44.45	49.00	49.00	49.00
0.4	20.66	20.66	21.83	21.83	21.83	40.44	40.46	43.87	43.87	43.89
0.5	19.66	19.73	20.89	20.88	20.89	38.84	38.65	41.45	41.45	41.52
0.6	18.09	18.20	19.30	19.29	19.30	38.60	38.32	40.93	40.93	41.03

Although the overall trend between natural frequency and delamination size showed good correlation between the FEM results and those taken from the literature, a larger discrepancy can be seen here than was present in the beam model verification. As described previously, this was to be expected, since the essential condition of L/H>10 was not respected for all beam segments in the delamination model, and the ANSYS® design of this system did not enforce rigid connectors at the delamination tips. Instead, soft connectors allowed the material to deform more naturally in the axial direction. This relaxation of imposed displacements meant that the overall stiffness of the system was reduced when compared to those systems designed with rigid connectors, such as the beam-based formulations. With a lower overall system stiffness, a reduction in the magnitude of the natural frequencies can be observed.

More detailed results concerning conditions not presented in the literature may be located in the internal report assembled by Johan Bellecave [11]. Effects of off-midplane and off-centre delaminations, as well as material property differences between the two layers are examined and various software protocols for the automatic generation of meshed geometry and results are presented, which were utilized during the course of this work.

5. Concluding Remarks

In the preceding, a detailed analysis of various important aspects of single- and double-delamination of layered beams was presented. Exact (analytical) solutions existed and were found for the simple cases here, and were compared with results obtained from traditional FEM, DSM and DFE formulations. DSM and DFE, by their frequency-dependent natures, provided excellent results compared to those found in the literature and from the other solution techniques, for a relatively coarse mesh size. It was shown that, using very few elements, even higher mode natural frequencies and mode shapes could be calculated with excellent precision. One of the drawbacks of the dynamic element-based techniques was that the root-finding algorithms used tended to be non-linear and difficult to compute fast, unless advanced techniques were used. Using a frequency sweep, natural frequencies could be found from the non-linear eigenproblem solution, but not as quickly as solving the linear eigenproblem that represents FEM free vibration analysis. However, this drawback was more than offset by both the use of advanced root-finding algorithms and by the inherent accuracy of the DSM and DFE formulations.

For double-delamination, since the same axial location would be shared by many elements, 2- and 3-node conventional FEM formulations were generated. This was done in an attempt to reduce the element count while retaining the accuracy of the model. It was found that the use of 3-node beam elements with quartic shape functions (as opposed to the more common Hermite cubic shape functions found in 2-node beams) did not produce significantly better results for the same mesh size. The difference was catalogued, though, and the exercise of generating and analyzing the system using different element types was well-served.

A verification of the models presented was carried out, in comparison with data available from a commercial finite element suite. The purpose of this was twofold: first, it would give another independent source of data to which comparisons were made, and second, it gave an insight into how accurate the existing engineering toolset was at analyzing the problem of delamination. Using a beam element model, and based on the documented convergence data, it was found that a fine mesh was required to accurately capture all of the

delamination effects. Most commercial FEM applications require quite fine mesh densities in order to produce accurate results with a high degree of convergence, especially for higher mode numbers. The opportunity to improve upon this was noted – using an extremely coarse (in comparison) DFE or DSM mesh, similar results could be obtained, without having to solve a large eigenproblem. Additionally, the ability to analyze any mode number using dynamic elements, regardless of the total number of degrees of freedom in the global system, is a clear advantage of the use of dynamic elements.

The 2-dimensional FEM model generated using the commercial finite element suite (ANSYS®) exhibited some interesting, but expected, trends. The trend was for the natural frequencies of the 2-dimensional model to be lower than that of an analytical model. On further inspection, the reasons for this discrepancy become clear, though. The 2-dimensional element model did not satisfy the essential condition of $L/H>10$ for all beam segments in the delamination model. In addition, it made no assumptions at the delamination faces – whereas the rigid connector assumption is one of the hallmarks of the beam-based solutions. The lack of rigid connectors, while potentially closer to the behaviour of a real delaminated system, meant that the system was less rigid. Hence, a reduction in stiffness led to lower natural frequencies.

It is clear from an examination of the literature that the direction most researchers, including Banerjee, are taking is toward the analysis of sandwich beams. The utility of a sandwich beam model lies in the coupling between various displacements and internal forces. Sandwich beams, which are regularly being used in structural applications, exhibit more complex behaviour than the homogeneous (or homogenized) beams analyzed here. Thus, it would be remiss to not pursue a detailed model of a delaminated sandwich beam in the future. Since the behaviour of sandwich beams is so much more complex, no analytical solutions are readily available for even the natural frequencies of intact beams. However, both DSM and DFE solutions do exist for the free vibration of intact sandwich beams. This means that, as presented here, an extrapolation of the intact beam solutions could be applied to model a delaminated beam. This would be a significant advancement in the analysis of delaminated beams.

Also, the techniques discussed here are not limited to beams. Although the formulations were carried out on beam structures, composite plates are seeing increased use in structural applications, especially in the aerospace industry, where their use is becoming more common in fuselage, wing, and stabilizer skins. Important in the aerospace industry as well is the use of composite materials in the fan and compressor sections of turbine motors. The complex geometry and material properties of these make them very difficult to analyze using existing techniques. With a robust dynamic delamination model, this could provide analysts with a powerful tool for analyzing the vibration of defective structures in such a high-stress environment.

6. List of Contributions

1. Erdelyi, N. and Hashemi, S.M. (2012). A dynamic stiffness element for free vibration analysis of delaminated layered beams. Modelling and Simulation in Engineering **vol. 2012**, Article ID 492415. doi:10.1155/2012/492415 (8 pp).

2. Erdelyi, N. and Hashemi, S.M. (2010). An Exact Dynamic Stiffness Matrix (DSM) Formulation for Free Vibration Analysis of Delaminated Beams. Proceedings of the 8th Joint Canada-Japan Workshop on Composite Materials, **July 28-31, 2010, Montreal, Canada** (10pp).

3. Erdelyi, N. and Hashemi, S.M. (2010). Free Vibration Analysis of Delaminated Layered Beams: A Dynamic Finite Element (DFE) Technique. Proceedings of the 8th Joint Canada-Japan Workshop on Composite Materials**, July 28-31, 2010, Montreal, Canada** (13pp).

4. Erdelyi, N. and Hashemi, S.M. (2011). A Dynamic Stiffness Matrix for the Free Vibration Analysis of Doubly Delaminated layered Beams. The 1st Int. on Acoustics and Vibration**, 21-22, 2011, Tehran, I-R-Iran.**

5. Erdelyi, N. and Hashemi, S.M. (2011). Vibration Modeling of Doubly Delaminated layered Beams. CD Proceedings of the 2nd Joint US/Canada Conference on Composites/26th ASC Annual Technical Conference**, September 26-28, 2011, Montreal, QC** (16 pp).

6. Erdelyi, N. and Hashemi, S.M. (2012). A dynamic finite element analysis of delaminated layered beams. Composite Structures, **Submitted** (24 pp).

7. References

1 Backstrom, D. and Nilsson, A.C. (2007). Modelling the Vibration of Sandwich Beams Using Frequency-dependent Parameters. *Journal of Sound and Vibration* **300**: 589-611.

2 Banerjee, J.R. and Williams, F.W. (1994). Coupled Bending-Torsional Dynamic Stiffness Matrix of an Axially Loaded Timoshenko Beam Element. *International Journal of Solids and Structures* **31**: 749-762.

3 Banerjee, J.R. and Williams, F.W. (1995). Free vibration of composite beams – an exact method using symbolic computation. *Journal of Aircraft* **32(3)**: 636-642.

4 Banerjee, J.R. (1997). Dynamic stiffness formulation for structural elements: A general approach. *Computers & Structures* **63 (1)**: 101-103.

5 Banerjee, J.R. (2003). Free vibration of sandwich using the dynamic stiffness method. *Computers & Structures* **81**, 1915-1922.

6 Banerjee, J. R. and Sobey, A.J. (2005). Dynamic stiffness formulation and free vibration analysis of a three-layered sandwich beam. *International Journal of Solids and Structures* **42**: 2181-2197.

7 Banerjee, J. R., Cheung, C.W., Morishima, R., Perera, M. and Njuguna, J. (2007). Free vibration of a three-layered sandwich beam using the dynamic stiffness method and experiment. *International Journal of Solids and Structures* **44**: 7543-7563.

8 Banerjee, J.R.**,** Su, H., and Jayatunga, C. (2008). A dynamic stiffness element for free vibration analysis of composite beams and its application to aircraft wings**.** *Computers & Structures* **86 (6)**: 573**–**579**.**

9 Banerjee, J.R. and Su, H. (2008). A New Method for Free Vibration of Beams using Theory of Elasticity. Proceedings of the *49th AIAA/ASME/ASCE/AHS/ASC Structures, Structural Dynamics, and Materials Conference*, April 7-10, Schaumburg, Illinois (22 pp).

10 Bathe, K-J. (1982). *Finite element procedures in Engineering analysis*, Prentice Hall.

11 Bellecave, J. (2010). Vibration Analysis of Defective Layered Beams. *Internal report, Department of Aerospace Engineering; Faculty of Engineering, Architecture and Science; Ryerson University*. Toronto, Ontario, September 2010

12 Borneman, S.R., Hashemi, S.M., and Alighanbari, H. (2008). Vibration Analysis of Doubly Coupled Cracked Composite Beams: An Exact Dynamic Stiffness Matrix. *International Review of Aerospace Engineering (I.RE.AS.E.)* **1(3)**: 298-309.

13 Brandinelli, L. and Massabo, R. (2003). Free Vibrations of Delaminated Beam-Type Structures with Crack Bridging. *Composite Structures* **61**: 129-142.

14 Della, C.N. and Shu, D. (2006). Vibration of Delaminated Multilayer Beams. *Composites: Part B- Engineering*, **37 (2-3)**: 227-236.

15 Della, C.N. and Shu, D. (2006). Free Vibration Analysis of Composite Beams with Overlapping Delaminations. *European Journal of Mechanics A/Solids* **24**: 491-503.

16 Della, C.N. and Shu, D. (2007). Vibration of Delaminated Composite Laminates: A Review. *Transactions of the ASME: Journal of Applied Mechanics* **60**: 1-20.

17 Della, C.N. and Shu, D. (2009). Free Vibration Analysis of Multiple Delaminated Beams Under Axial Compressive Load. *Journal of Reinforced Plastics and Composites* **28**:1365-1381.

18 Doxsee, L.E., Rubbrecht, P., Li, L., Verpoest, I. and Scholle, M. (1993). Delamination Growth in Composite Plates Subjected to Transverse Loads. *Journal of Composite Materials* **27**: 764-781.

19 Hashemi, S.M. (1998). Free Vibrational Analysis of Rotating Beam-like Structures: A Dynamic Finite Element Approach. *Ph.D Thesis, Department of Mechanical Engineering, Laval University, Québec, Canada.*

20 Hashemi, S.M. and Roach, A. (2005). A Dynamic Finite Element for Vibration Analysis of Composite Circular Tubes, in the Proceedings of the *10th International Conference on Civil, Structural and Environmental Engineering Computing*, B.H.V. Topping, (Editor), Civil-Comp Press, Stirlingshire, UK, Paper 177, 2005. doi:10.4203/ccp.81.177, Rome, Italy, 30 August-2 September.

21 Hashemi, S.M. and Roach, A. (2010). A Dynamic Finite Element for the Free Vibration Analysis of Extension-Torsion Coupled Composite Beams. *Mathematics in Engineering, Science and Aerospace (MESA)*, *THE TRANSDISCIPLINARY INTERNATIONAL JOURNAL*, **1(3)**: 221-239.

22 Hashemi, S.M., and Adique, E.J. (2010). A Quasi-Exact Dynamic Finite Element for Free Vibration Analysis of Sandwich Beams. *Applied Composite Materials* **17:** 259-269

23 Hein, H. (2006). The Influence of Delamination of Free Vibrations of Composite Beams on Pasternak Soil. *Proceedings of the Estonian Academy of Sciences. Physics. Mathematics* **55(4)**: 220-234.

24 Hu, J. S. and Hwu, C. (1995). Free Vibration of Delaminated Composite Sandwich Beams. *AIAA Journal* **33(10)**: 1911-1918.

25 Krawczuk, M., Ostachowicz, W. and Zak, A. (1997). Dynamics of Cracked Composite Material Structures. *Computational Mechanics* **20**: 79-83.

26 Krawczuk, M., Ostachowicz, W. and Zak, A. (2000). Numerical and Experimental Investigation of Free Vibration of Multilayer Delaminated Composite Beams and Plates. *Computational Mechanics* **26**: 309-315.

27 Kudela, P. and Ostachowicz, W. (2009). A Multilayer Delaminated Composite Beam and Plate Elements: Reflections of Lamb Waves at Delamination. *Mechanics of Advanced Materials and Structures* **16(3)**: 174-187.

28 Lee, J. (2000). Free vibration analysis of delaminated composite beams. *Computers & Structures* **74(2)**: 121-129.

29 Lee, S., Park, T., and Voyiadjis, G. Z. (2002). Free Vibration Analysis of Axially Compressed Composite Beam-Columns with Multiple Delaminations. *Composites Part B: Engineering* **33**: 605-617.

30 Lee, S., Park, T., and Voyiadjis, G. Z. (2003). Vibration Analysis of Multi-Delaminated Beams. *Composites Part B: Engineering* **34**: 647-659.

31 Lestari, W. and Hanagud, S. (1999). Health Monitoring of Structures: Multiple Delamination Dynamics in Composite Beams. *Report for American Institute of Aeronautics and Astronautics* **AIAA-99-1509**.

32 Liu, M. and Yu, J. (2003). Finite Element Modeling of Delamination by Layerwise Shell Element Allowing for Interlaminar Displacements. *Composites Science and Technology* **63**: 517–529.

33 Logan, D.L. (2007). *A First Course in the Finite Element Method, Fourth Edition*. Toronto, ON: Nelson.

34 Luo, H. and Hanagud, S. (2000). Dynamics of Delaminated Beams. *International Journal of Solids and Structures* **37**: 1501-1519.

35 Mujumdar, P. and Suryanarayan, S. (1988). Flexural Vibrations of Beams with Delaminations. *Journal of Sound and Vibration* **125**: 441-461.

36 Ostachowicz, W. and Zak, A. (2004). Vibration of a Laminated Beam with a Delamination Including Contact Effects. *Shock and Vibration* **11**: 157-171.

37 Perel, V. Y. (2005). Finite Element Analysis of Vibration of Delaminated Composite Beam with an Account of Contact of the Delamination Crack Faces, Based on the First-order Shear Deformation Theory. *Journal of Composite Materials* **39**: 1843-1876.

38 Rao, P.M., Wenge, T. and Shu, D. (2005). Buckling Analysis of Tri-Layer Beams with Enveloped Delaminations. *Composites Part B: Engineering* **36**: 33-39.

39 Roche, C.H. and Accorsi, M.L. (1998). A newfinite element for global modeling of delaminations in laminated beams. *Finite Elements in Analysis and Design* **31**:165-177.

40 Sankar, B.V. (1991). A Finite Element for Modelling Delamination in Composite Beams. *Computers & Structures* **38(2)**: 239-246.

41 Schnabl, S., Saje, M., Turk, G. and Planinc, I. (2007). Locking-Free Two-Layer Timoshenko Beam Element with Interlayer Slip. *Finite Elements in Analysis and Design* **43**: 705-714.

42 Schwarts-Givli, H., Rabinovitch, O. and Frostig, Y. (2007). Free Vibrations of Delaminated Unidirectional Sandwich Panels with a Transversely Flexible Core – A Modified Galerkin Approach. *Journal of Sound and Vibration* **301**: 253-277.

43 Shen, M.H. and Grady, J.E. (1992). Free Vibrations of Delaminated Beams. *AIAA Journal* **30(5)**: 1361-1370.

44 Shu, D. (1995). Vibration of Sandwich Beams with Double Delaminations. *Composites Science and Technology* **54**: 101-109.

45 Shu, D. and Fan, H. (1996). Free Vibration of Bimaterial Split Beam. *Composites Part B: Engineering* **27**: 79-84.

46 Swannell, P. (1973). The automatic computation of natural frequencies of structural frames using an exact matrix technique. *Theory and practice in finite element structural analysis*, *Proceedings of the 1973 Tokyo Seminar on Finite Element Analysis*; pp. 289-301.

47 Tracy, J. J. and Pardoen, G. C. (1989). Effect of Delamination on the Natural Frequencies of Composite Laminates. *Journal of Composite Materials* **23(12)**: 1200-1216.

48 Valvo, P. S. (2009). A Beam-Theory Based Method to Partition Fracture Modes in Delaminated Beams. *Proceedings of the XIX Congresso AIMETA*, September 14-17, Ancona, Italy (10 pp.)

49 Wang, J., Liu, Y., and Gibby, J. (1982). Vibrations of Split Beams. *Journal of Sound and Vibration* **84**: 491-502.

50 Wang K. (2004). *Vibration Analysis of Cracked Composite Bending-torsion Beams for Damage Diagnosis*. PhD Dissertation, Dept. Mech. Eng., Virginia Tech., Blacksburg, VA; http://scholar.lib.vt.edu/theses/available/etd-12032004-110007/.

51 Wang, K., Inman, D.J., and Farrar, C.R. (2005). Modeling and Analysis of Cracked Composite Cantilever Beam Vibrating in Coupled Bending and Torsion. *Journal of Sound and Vibration* **284**: 23-49.

52 Williams, F.W. and Wittrick, W.H. (1970). An automatic computational procedure for calculating natural frequencies of skeletal structures. *Int. J. of mech. Sci.* **12**:781-791.

53 Wittrick, W.H. and Williams, F.W. (1971). A General Algorithm for Computing Natural Frequencies of Elastic Structures. *Quarterly Journal of Mechanics and Applied Mathematics* **24:** 263-284.

54 Zou, Z., Reid, S.R., Li, S., Soden, P.D. (2002). Application of a Delamination Model to Laminated Composite Structures. *Composite Structures* **56**:375-389.

Appendix A: Mode Shapes of Double-Delaminated Beams

Model 1, from Chapter 3;

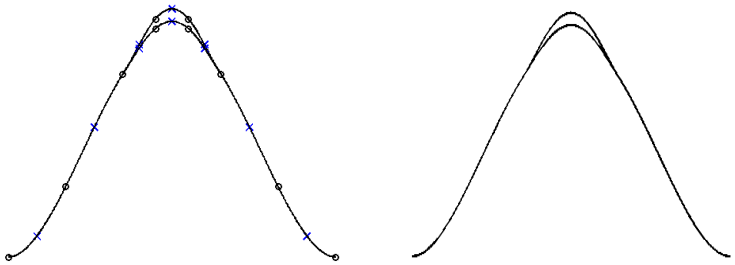

Figure 19 - mode 1, a/L = 0.3

Left: 3-node beam element, nodes visualized; Right: Analytical solution

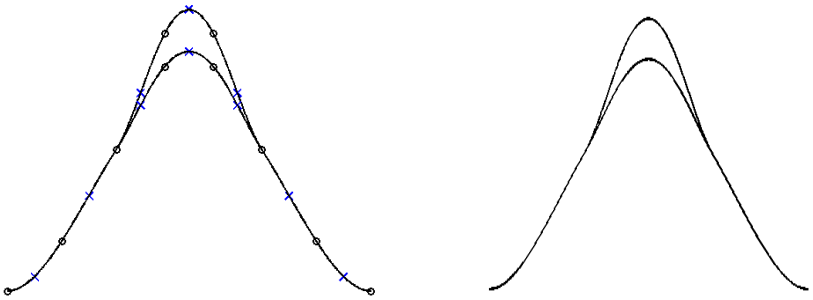

Figure 20 - mode 1, a/L = 0.4

Left: 3-node beam element, nodes visualized; Right: Analytical solution

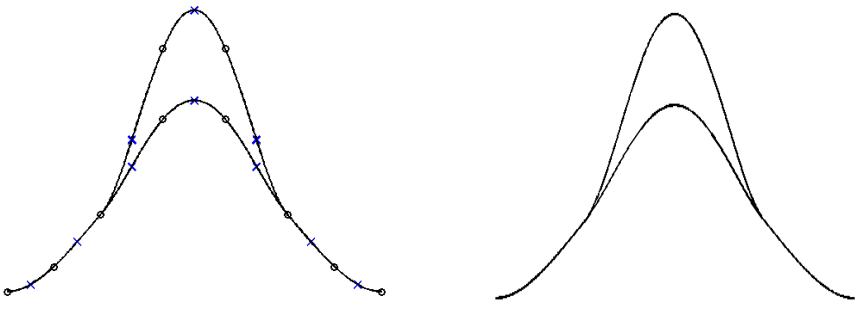

Figure 21 - mode 1, a/L = 0.5

Left: 3-node beam element, nodes visualized; Right: Analytical solution

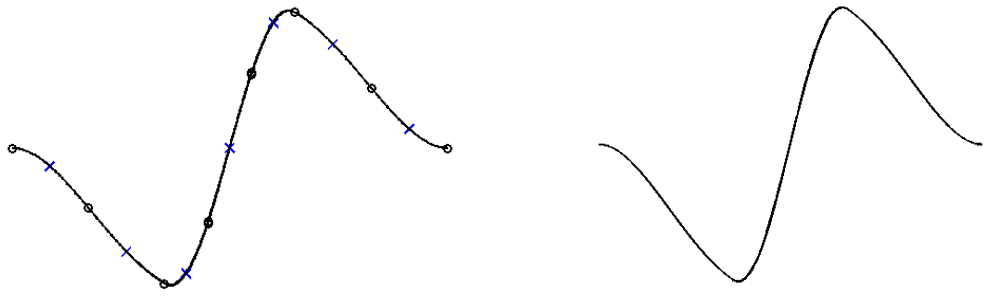

Figure 22 - mode 2, a/L = 0.3

Left: 3-node beam element, nodes visualized; Right: Analytical solution

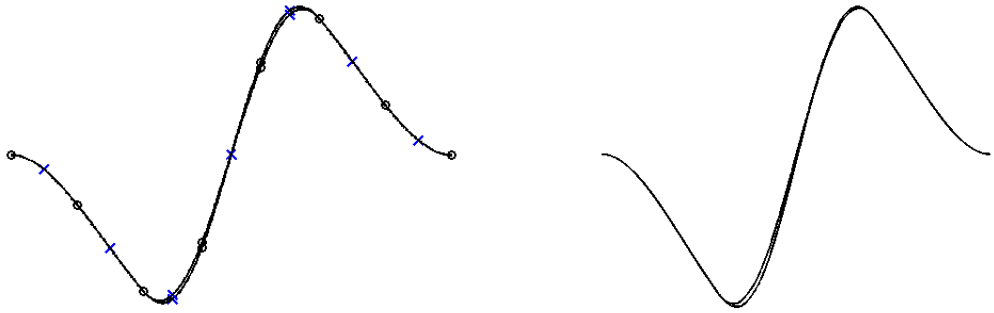

Figure 23 - mode 2, a/L = 0.4

Left: 3-node beam element, nodes visualized; Right: Analytical solution

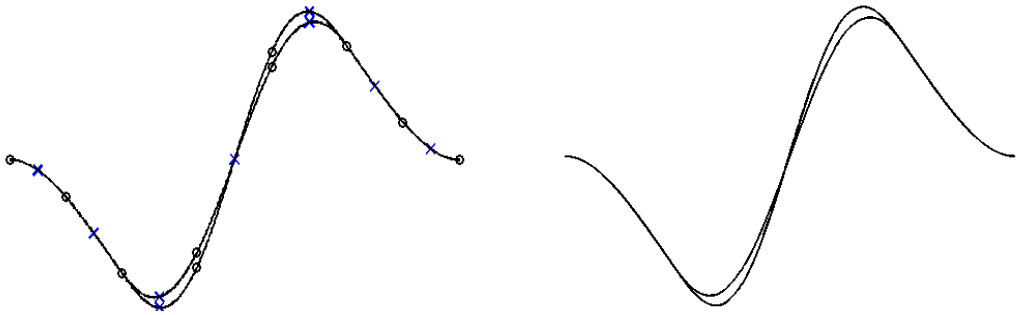

Figure 24 - mode 2, a/L = 0.5

Left: 3-node beam element, nodes visualized; Right: Analytical solution

Model 2, from Chapter 3;

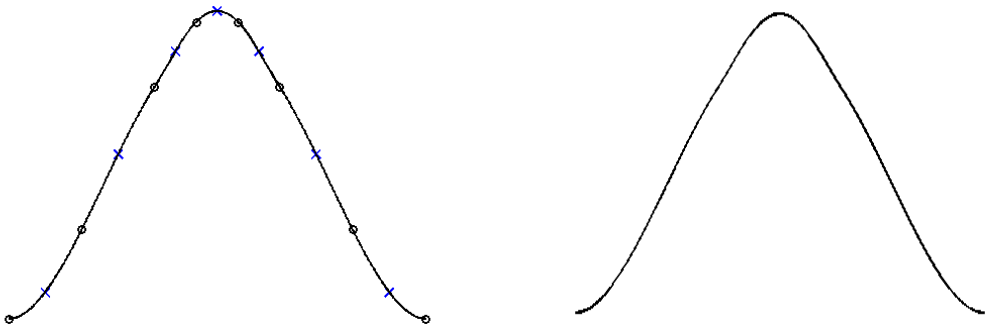

Figure 25 - mode 1, a/L = 0.3

Left: 3-node beam element, nodes visualized; Right: Analytical solution

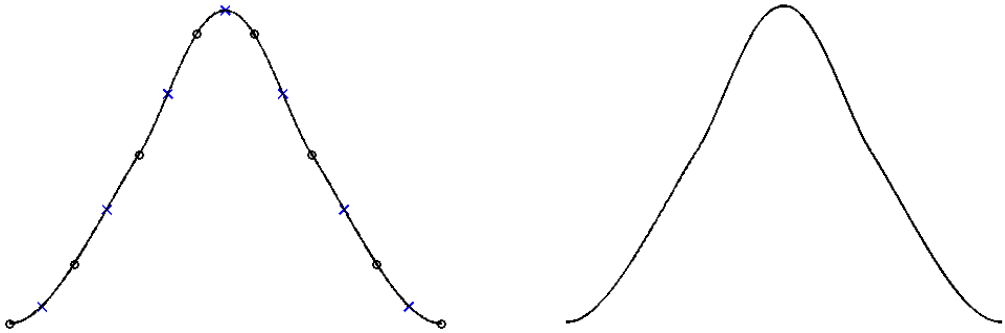

Figure 26 - mode 1, a/L = 0.4

Left: 3-node beam element, nodes visualized; Right: Analytical solution

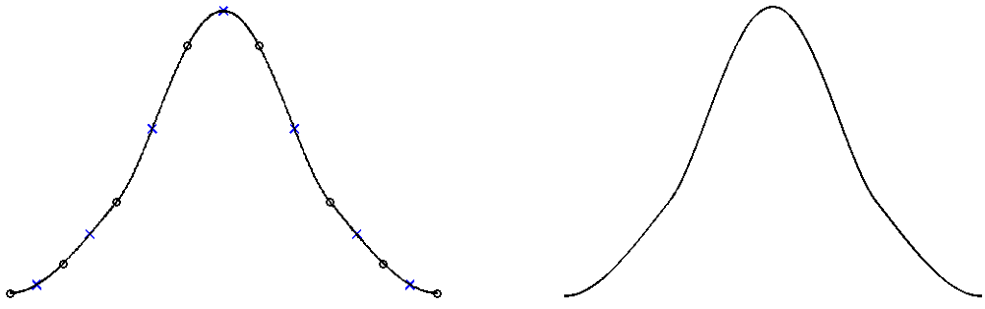

Figure 27 - mode 1, a/L = 0.5

Left: 3-node beam element, nodes visualized; Right: Analytical solution

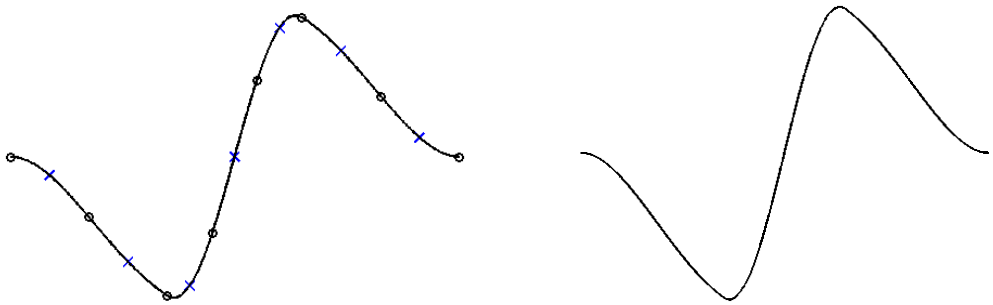

Figure 28 - mode 2, a/L = 0.3

Left: 3-node beam element, nodes visualized; Right: Analytical solution

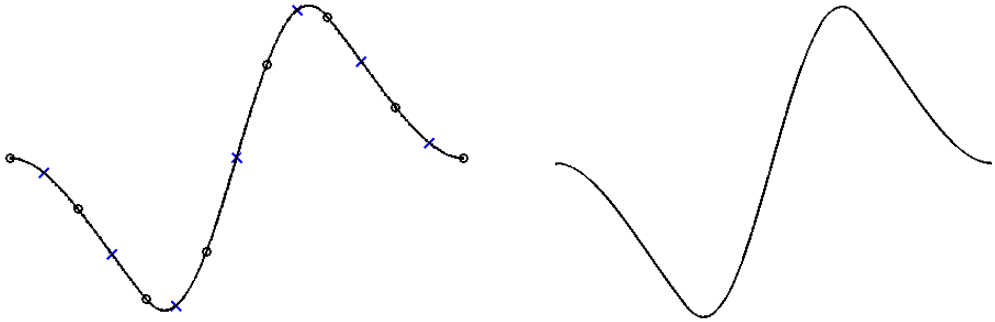

Figure 29 - mode 2, a/L = 0.4

Left: 3-node beam element, nodes visualized; Right: Analytical solution

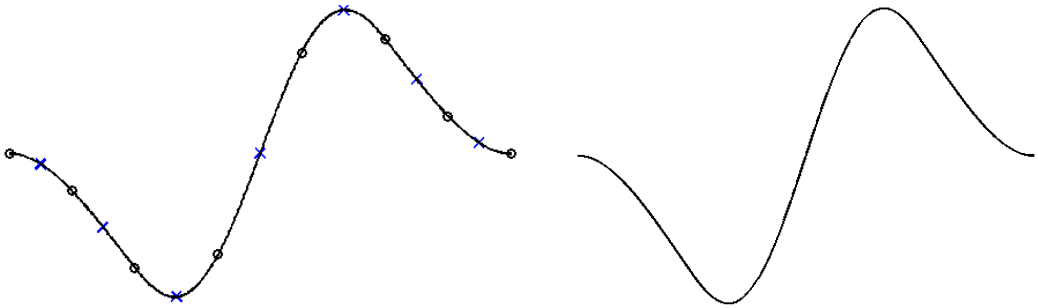

Figure 30 - mode 2, a/L = 0.5

Left: 3-node beam element, nodes visualized; Right: Analytical solution

Appendix B: Shape Functions

Quartic Shape Functions

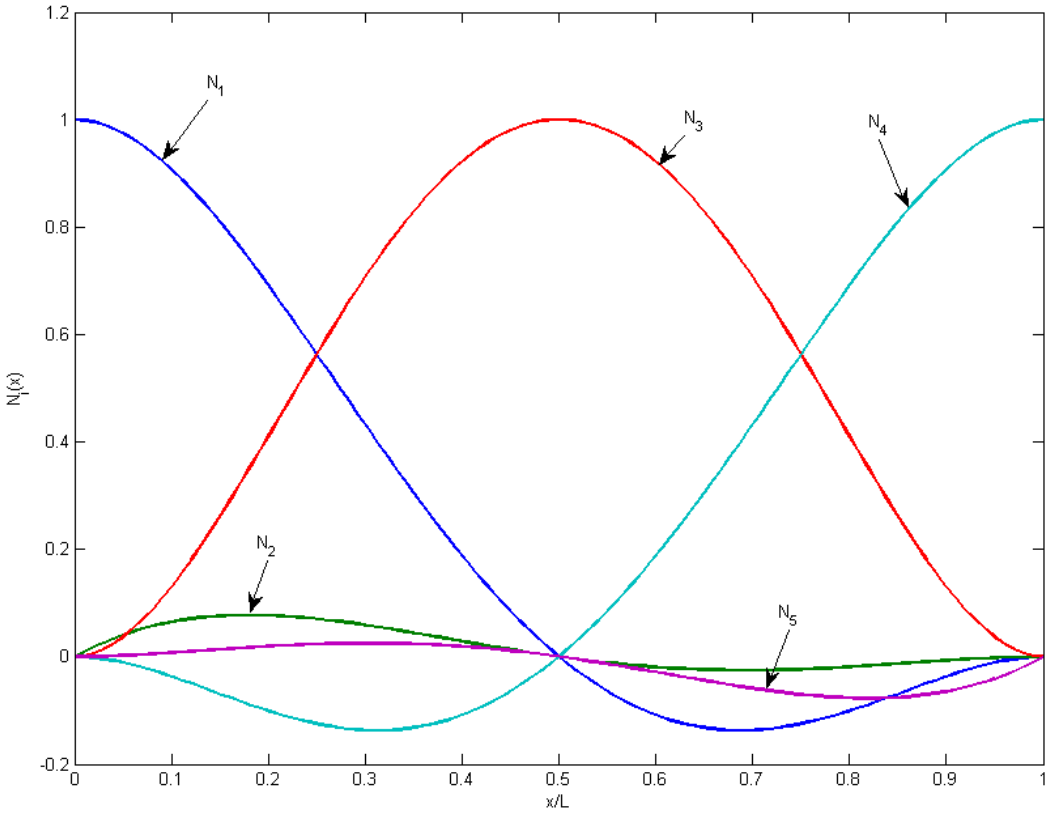

Figure 31 – Quartic shape functions used for double-delamination case study

$$N_1 = \frac{1}{L^4}(L-x)^2(L-2x)(L+4x)$$

$$N_2 = \frac{1}{L^3}x(L-x)^2(L-2x)$$

$$N_3 = \frac{1}{L^4}16x^2(L-x)^2$$

$$N_4 = -\frac{1}{L^4}x^2(L-2x)(5L-4x)$$

$$N_5 = \frac{1}{L^3}x^2(L-2x)(L-x)$$

Dynamic Shape Functions

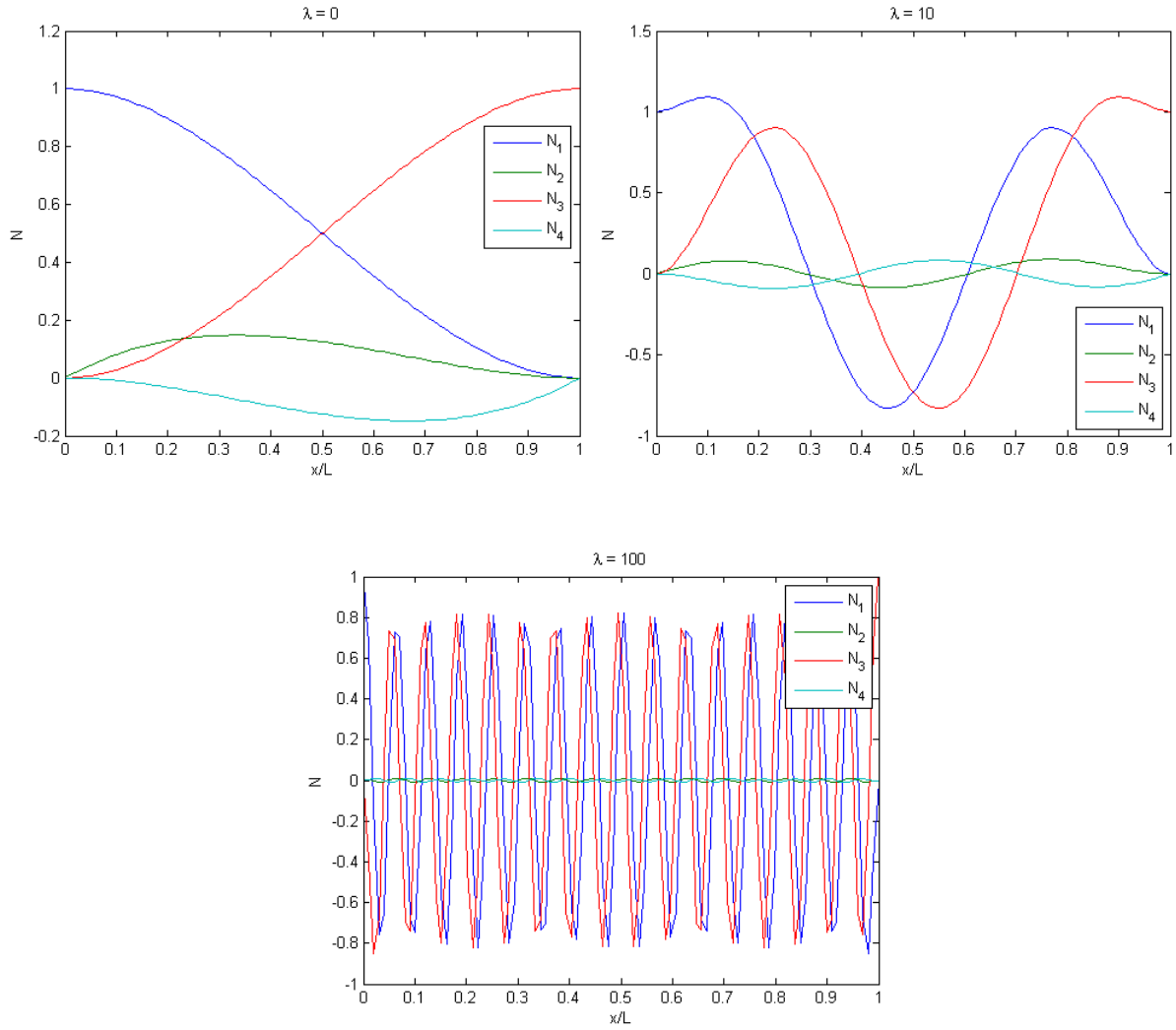

Figure 32 – Dynamic shape functions for different non-dimensional frequencies.
Top Left: Hermite cubic shape functions, *λ* -> 0;
Top Right: DFE shape functions, *λ* = 10; Bottom: DFE shape functions, λ = 100

$$\langle N \rangle = \langle N_1 \quad N_2 \quad N_3 \quad N_4 \rangle$$

$$N_1 = \frac{1}{DEN}\left[-\cos\left(\lambda\frac{x}{L}\right) + \sinh(\lambda)\sin\left(\lambda\left(\frac{x}{L}-1\right)\right) + \cosh(\lambda)\cos\left(\lambda\left(\frac{x}{L}-1\right)\right) + \cos(\lambda)\cosh\left(\lambda\left(\frac{x}{L}-1\right)\right) - \cosh\left(\lambda\frac{x}{L}\right) - \sin(\lambda)\sinh\left(\lambda\left(\frac{x}{L}-1\right)\right)\right]$$

$$N_2 = \frac{L}{\lambda}\frac{1}{DEN}\left[\cosh(\lambda)\sin\left(\lambda\left(\frac{x}{L}-1\right)\right) + \sinh(\lambda)\cos\left(\lambda\left(\frac{x}{L}-1\right)\right) - \sin\left(\lambda\frac{x}{L}\right) + \sin(\lambda)\cosh\left(\lambda\left(\frac{x}{L}-1\right)\right) + \cos(\lambda)\sinh\left(\lambda\left(\frac{x}{L}-1\right)\right) - \sinh\left(\lambda\frac{x}{L}\right)\right]$$

$$N_3 = \frac{1}{DEN}\left[\cos\left(\lambda\frac{x}{L}\right)\cosh(\lambda) - \cos\left(\lambda\left(\frac{x}{L}-1\right)\right) - \sin\left(\lambda\frac{x}{L}\right)\sinh(\lambda) - \cosh\left(\lambda\left(\frac{x}{L}-1\right)\right) + \cosh\left(\lambda\frac{x}{L}\right)\cos(\lambda) + \sinh\left(\lambda\frac{x}{L}\right)\sin(\lambda)\right]$$

$$N_4 = \frac{L}{\lambda}\frac{1}{DEN}\left[-\cos\left(\lambda\frac{x}{L}\right)\sinh(\lambda) - \sin\left(\lambda\left(\frac{x}{L}-1\right)\right) + \sin\left(\lambda\frac{x}{L}\right)\cosh(\lambda) - \sinh\left(\lambda\left(\frac{x}{L}-1\right)\right) - \cosh\left(\lambda\frac{x}{L}\right)\sin(\lambda) + \sinh\left(\lambda\frac{x}{L}\right)\cos(\lambda)\right]$$

$$DEN = 2(\cos(\lambda)\cosh(\lambda) - 1)$$

Appendix C: Double-Delamination Mesh Sensitivity Analysis

Mesh sensitivity analyses were undertaken for each beam element for the delamination configuration shown in the previous section. The different meshing schemes outlined below were used to determine an appropriate element size for approximate convergence. Convergence will be estimated using the first three fundamental frequencies in each case. Note the boundary conditions are clamped-clamped.

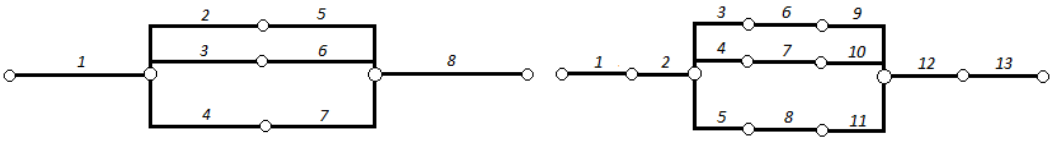

Figure 33 –Left- configuration 1; Right- configuration 2

The element configurations and numbering schemes for each mesh

In addition, the following delamination parameters will be chosen, and assumed constant for the purposes of evaluating mesh sensitivity, and will be varied in the actual analysis to follow:

Delamination Length	0.2L
H_2	$0.3H_1$
H_3	$0.2H_1$

2-Node Beam

Table 9 – 2-node beam sensitivity analysis

	Configuration 1	*Configuration 2*	*Exact (Analytical)*
$\boldsymbol{\lambda_1}$	4.7312	4.7296	4.7250
$\boldsymbol{\lambda_2}$	7.3775	7.2563	7.2450
$\boldsymbol{\lambda_3}$	10.6919	10.3695	10.3350

While it can be seen that all 3 fundamental frequencies do approximately converge (error less than 1%) for the second configuration, the maximum error for the first configuration, using 2-node beam elements, is approximately 3.4%. While still within a reasonable margin of

error, it will now be investigated if increasing the order of the interpolation function positively affects this result.

3-Node Beam

Table 10 – 3-node beam sensitivity analysis

	Configuration 1	*Configuration 2*	*Exact (Analytical)*
$\boldsymbol{\lambda_1}$	4.7239	4.7243	4.7250
$\boldsymbol{\lambda_2}$	7.2468	7.2510	7.2450
$\boldsymbol{\lambda_3}$	10.3384	10.3437	10.3350

Based on error between configurations, convergence was achieved to within 1% of the analytical solution, using configuration 1 for a 3-node beam element. The benefit of utilizing more elements has not been shown here, and solution times could be reduced by using configuration 1 due to the reduction in elements from 13 to 8 (38% reduction) and reduction in nodes from 25 to 15 (40% reduction), with no appreciable loss in solution accuracy. Additionally, given the nature of DFE development, as opposed to traditional FEM development, the number of natural frequencies and mode shapes available for a given mesh is not dependent on the number of elements used. Frequency sweeps or more advanced root finding algorithms are not limited to the degree of freedom count as an eigensolution is, so long as the frequency range being analyzed does not cause a computational floating-point overflow.

It can also be observed that, while slightly higher accuracy was obtained using the 3-node beam element - as expected - this increase was only marginal for the first two fundamental modes. Therefore, no absolute rule can be established as to which element is better suited for all situations. In fact, the situation itself would likely dictate which element to select - smaller problems benefiting from the increased accuracy of the 3-node element and large problems benefiting from the increased solution efficiency of the 2-node element (due to a 20% reduction in degrees of freedom per element).